Chapter 2

Results from the Hydrodynamic Element of the 1994 Entrapment Zone Study in Suisun Bay

By Jon R. Burau, Jeffrey W. Gartner, and Mark Stacey
U.S. Geological Survey
Placer Hall, 6000 J Street
Sacramento, Ca 95819-6129

Abstract

The term entrapment zone has been used to describe a zone of elevated concentrations of particles, plankton, and juvenile fish observed in low-salinity areas of north (San Francisco) bay and the western Sacramento-San Joaquin Delta, California. The hypothesized mechanism for entrapment was a combination of particle aggregation, sinking and a residual current null zone. The null zone is a time-mean, near-bed flow convergence where riverine flow ends and gravitational circulation begins that was presumed to occur near a salinity of 2 psu. Current-meter measurements made prior to 1990 provide evidence of gravitational circulation and a null zone during autumn in the north bay of San Francisco Bay, including Suisun Bay and the western delta. Data collected after 1990, however, show an absence of gravitational circulation from most of Suisun Bay during spring, and the presence of multiple gravitational circulation cells between bathymetric constrictions elsewhere in the bay. Because null zones appear to be bathymetrically controlled, they often occur in areas far removed from the low salinity zone (near X2, the position of a bottom salinity of 2 psu). The presence or absence of gravitational circulation can be predicted with appropriate physical scaling, which explains the most recent and historical current-meter observations throughout the Bay/Delta system. In areas where gravitational circulation is weak or nonexistent, some other physical or biological mechanism(s) must be causing the observed concentration of particles and organisms in the low-salinity zone. Four physical mechanisms are discussed in this chapter: density-current pulses that occur near slack tide, ebb/flood shear stress asymmetries, vertical migration of organisms during the tidal cycle, and an upstream mass flux known as Stokes' drift. Stokes' drift was eliminated from further consideration because variations in sea level are small relative to the mean depth and because of the weak correlation between sea level and the tidal currents in Suisun Bay.

Introduction

From a broad perspective the studies described in this report are meant to uncover the underlying processes that cause the observed accumulations of suspended particulate matter and organisms in the low salinity zone in San Francisco Bay. Many possible accumulation mechanisms in estuarine systems have been discussed in the literature that rely on the complex interaction between the tides, tidal currents, salt field, freshwater inflow, and biological behaviors at the tidal and residual timescales. Among them are: (1) gravitational circulation (Nichols and Poor 1967);

(2) shallow/channel exchange (Weir and McManus 1987); (3) wind-wave resuspension (Weir and McManus 1987); (4) stratification (Geyer 1993); (5) baroclinic flows that occur near slack water (Monismith and others 1996); (6) ebb/flood near-bed shear stress asymmetries (Stacey 1996); (7) ebb/flood vertical mixing asymmetries (Stacey 1996); (8) local minimums in energy [actually local energy flux divergence minimums] (Jay and others 1990); and finally (9) vertical or lateral migration (Kimmerer and Bennett, this volume).

In the San Francisco estuary, a gravitational-circulation based conceptual model of entrapment (Figure 2-1) has prevailed for the last few decades that was essentially borrowed from the other estuaries (Chesapeake: Pritchard 1952; Schubel 1968. Thames River: Ingles and Allen 1957. Mersey estuary: Bowden 1960) and was confirmed in a limited way in San Francisco Bay using (1) current meter data [Peterson and others (1975); Walters and Gartner (1985); Mortenson (1987); Smith (1987); and Nichol (1996)] and (2) drifter studies (Conomos and others 1971).

The data collected as part of the entrapment zone studies suggest, however, a more complicated picture of the residual currents than is shown in Figure 2-1. The actual residual currents differ from this simplistic conceptual model because of the complex interaction between the seasonal landward migration of the salt field (in particular, the position of the horizontal salinity gradient) with the spatially variable geometry of north bay (a region including San Pablo Bay, Carquinez Strait, and Suisun Bay; Figure 2-2) and vertical mixing caused by the tidal currents. The idea that an estuarine turbidity maximum occurs in the low-salinity zone that is directly derived from gravitational circulation (Figure 2-1) is useful because, based on the analysis of these data, this model applies in certain reaches of north bay (for example, seaward of Pinole Shoal and in Carquinez Strait) and in the western delta.

However, Figure 2-1 may be incorrectly interpreted to mean gravitational circulation directly advects nutrients and biota, somewhat like a conveyor belt, from the Pacific Ocean through north bay into the low salinity zone. What the data in this chapter suggest instead is that gravitational circulation is rare in parts of the estuary (for example, the ship channel in Suisun Bay), and when gravitational circu-

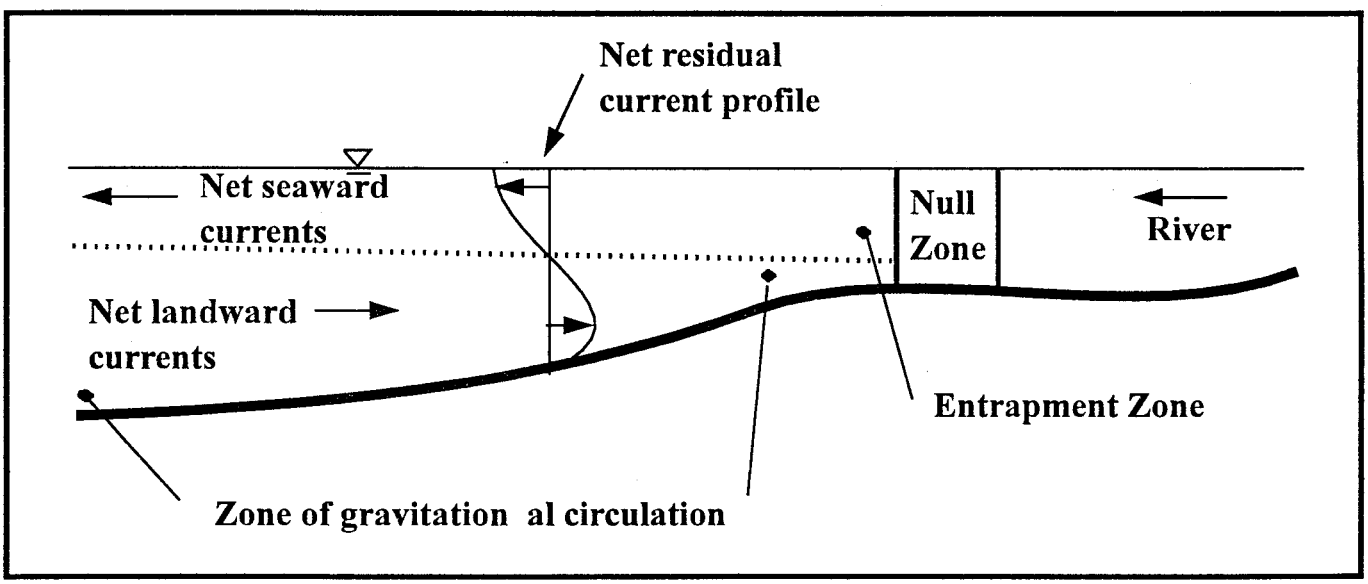

Figure 1
CONCEPTUAL MODEL OF THE ENTRAPMENT AND NULL ZONES

lation does occur, it exists as a series of cells (bounded at either end by sills) whose strength varies seasonally with the salt field.

Finally, because analysis of these data suggests that gravitational circulation is not as strong nor as pervasive as once thought, alternate mechanisms are being considered that could substantially contribute to the observed accumulations in certain reaches of north bay (Kimmerer and Bennett, this volume). One expects, however, that because the strength of gravitational circulation is primarily controlled by the position of the salt field and secondarily by the strength of the local tidal currents, the relative contributions from alternate accumulation mechanisms will also change as a function of these processes. For example, because gravitational circulation appears to dominate residual transport in Carquinez Strait, the contribution of gravitational circulation to accumulations in the low salinity zone will likely dominate any other, more subtle mechanisms when the low salinity zone is in Carquinez Strait.

On the other hand, the analysis of the data described in this chapter suggests that gravitational circulation is rare in the ship channel of Suisun Bay; therefore, if a turbidity maximum or biological maximum exists in this reach, other accumulation mechanisms must be making a substantial contribution. Therefore, any useable conceptual model of accumulation in the low salinity zone, if it is true to the physics, will have a seasonal component (position of the salt field) that depends on the hydrology in

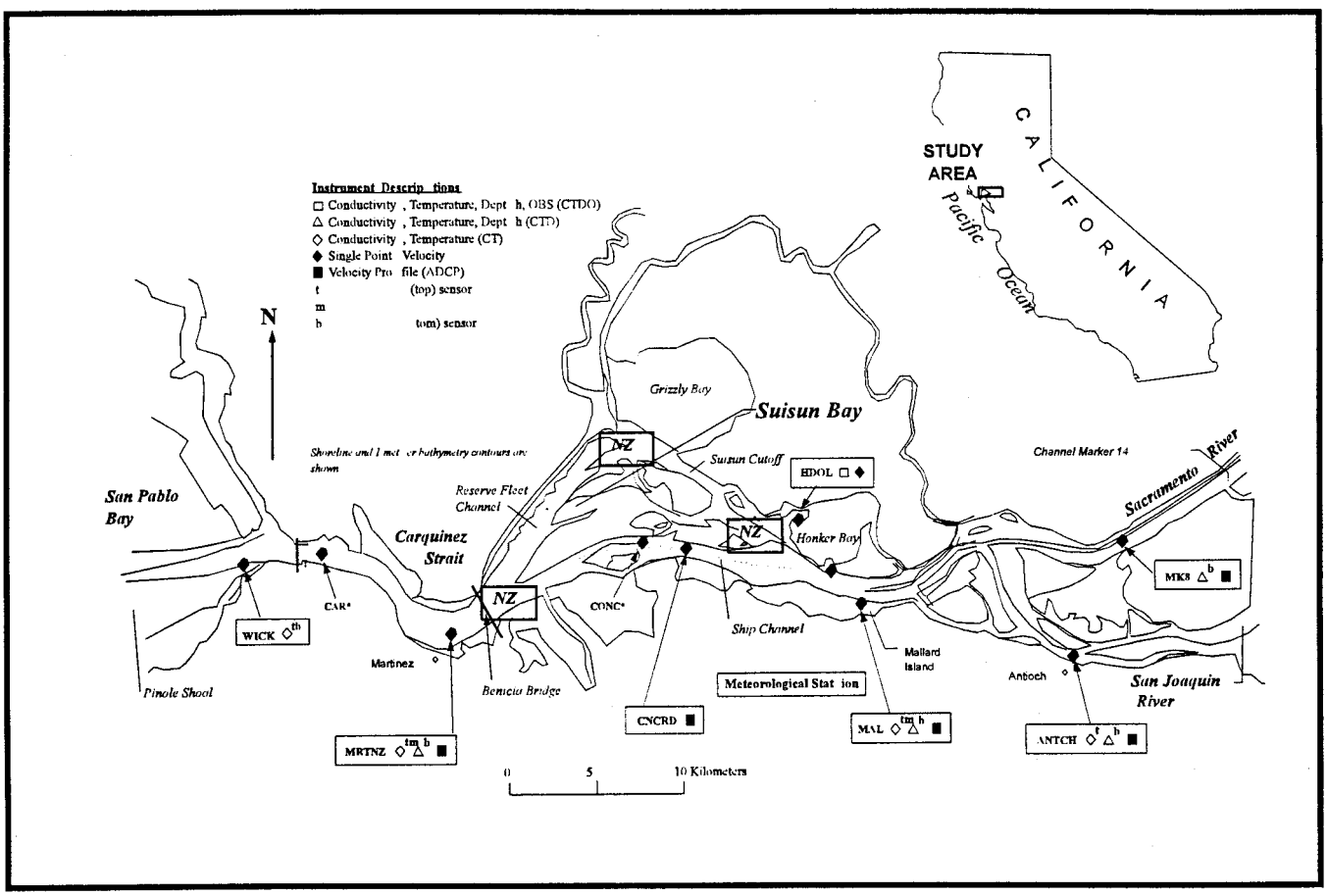

Figure 2
APPROXIMATE 1994 ENTRAPMENT ZONE STUDY *IN SITU* INSTRUMENT POSITIONS, NORTH SAN FRANCISCO BAY
Null zone symbol (NZ) shows potential null zone location.
National Oceanographic and Atmospheric Administration deployments in 1992 are denoted with an *.

a given year and a component dependent on location in the estuary (bathymetry).

This chapter presents results of the analyses of U.S. Geological Survey (USGS) hydrodynamic data collected as part of the 1994 Interagency Ecological Program (IEP) entrgpment zone study. The USGS took part in three 30-hour cruises in the north bay between April and June 1994. Prior to these cruises, *in situ* instruments that measured currents and salinity were deployed. This chapter focuses primarily on the analysis of data from five acoustic Doppler current profilers (ADCPs) deployed in Carquinez Strait, Suisun Bay, and the western delta (Figure 2-2). These analyses suggest a revision of the conceptual model of the entrapment zone. In this chapter, the existing conceptual model of entrapment based on a gravitational circulation hypothesis is discussed, and data inconsistent with this conceptual model are presented. A revised conceptual model of gravitational circulation based on the horizontal Richardson number is presented.

This revised model is consistent with the hydrodynamic data collected to date. Because the net currents in the channels cannot explain the observed accumulation of suspended sediment (based on secchi disk data) and various organisms in the low salinity zone (–2 psu), alternate, tidal timescale, hydrodynamic (biological) processes were considered. (Salinities in this chapter's figures are given without units because, by definition, salinity is a conductivity ratio that has no physical units (Millerno 1993). For salinities greater than 2 psu, salinity is computed on the basis of the UNESCO standard (UNESCO 1985). Salinities less than 2 psu are computed after Hill and others (1986)). The lateral variation in the tides and tidal currents and the storage and release of waters into and out of the shallows substantially contribute to the distributions of salinity, suspended-sediment concentrations, and of nonmotile and feebly-swimming biota throughout the estuary. These processes, however, are beyond the scope of this chapter. This chapter focuses on three possible accumulation processes that act in the vertical plane: the first two processes involve the timing and structure of the velocity shear and vertical salinity stratification, and the third process examined is Stokes' drift.

Historical Perspective

Much of the conceptual understanding of the physics of the north bay was either inferred from detailed investigations of other estuaries or based on the velocity studies of Peterson and others (1975) and on the drifter studies of Conomos and others (1971). Peterson analyzed velocity measurements taken at eight stations throughout the estuary from 1956 to 1969. The measurements were taken at five depths during roughly 25-hour periods with Price AA[1] current meters. Based on these limited data, Peterson showed that gravitational circulation existed seaward of Carquinez Strait. Conomos and others (1971) clearly show that gravitational circulation moved drifters released offshore (a drifter is a device designed to move with the current, often at preset density) landward into the bay. However, we now know that the residual currents seaward of Carquinez Strait are not indicative of the residual currents in the north bay as a whole, and the drifter studies provided little in-

1 Use of the brand name in this chapter is for identification only and does not constitute endorsement by the U.S. Geological Survey.

sight into the residual current patterns in Suisun Bay because no drifters were recovered landward of Carquinez Strait.

The USGS (Cheng and Gartner 1984), in collaboration with the National Oceanic Atmospheric Administration (NOAA) collected 'large amounts of current data throughout San Francisco Bay (Denton and Hunt 1986), including the north bay. Although these records were generally short (<1 month) relative to the typical deployment length of today (~3 months) and were collected during various times of the year, Smith (1987) analyzed these data for the presence of gravitational circulation and concluded that gravitational circulation is a dominant feature seaward of the null zone. Walters and Gartner (1985) analyzed a subset of these data collected during autumn 1978 and found strong gravitational circulation [~ 15 centimeters per second (cm/s)] in Suisun Cutoff and weak gravitational circulation (<10 cm/s) at Mallard Island, in the Reserve fleet channel, and in Carquinez Strait. In autumn 1986, Mortenson (1987) collected a remarkably complete data set in Suisun Bay following a relatively small runoff event [~21,000 cubic feet per second (cfs)]. The residual currents measured by Mortenson showed a gravitational circulation cell in Suisun Cutoff during the falling limb of the hydrograph, a time when the horizontal salinity gradient was likely compressed and probably centered in the Suisun Cutoff area. Monismith and others (1996) confirm the observations made by Peterson and others (1975) and Cheng and Gartner (1984) that gravitational circulation dominates the residual flows in Carquinez Strait. Finally, data collected in the lower Sacramento River by the U.S. Army Corps of Engineers show a weak gravitational circulation cell in the western delta when salinities locally exceeded ~2 psu (Nichol 1996).

Therefore, ample hydrodynamic evidence existed in support of a gravitational-circulation-based conceptual model of entrapment until 1993, when the USGS, in collaboration with Stanford University, began an annual series of detailed hydrodynamic studies in Suisun Bay. The methodology and purpose of these investigations were consistent with the work of Peterson and others (1975), Cheng and Gartner (1984), Mortenson (1986), and Nichol (1996). The only significant improvement on the previous studies was in the sophistication and amount of oceanographic equipment used. ADCPs that can measure a complete velocity profile of as much as 0.5-meter (m) intervals and Conductivity-Temperature-Depth (CTDs) sensors, capable of being continuously and autonomously deployed for as long as 3 months, were simultaneously deployed to capture the temporal and spatial variability in the tidal and residual currents in Suisun Bay.

Definitions

A review of the entrapment zone literature (primarily U.S. Bureau of Reclamation or California Department of Water Resources reports) suggests that confusion exists about the definition of the entrapment zone (Arthur and Ball 1979; Kimmerer 1993). Although Kimmerer (1993) rigorously defines the entrapment zone as "the area of the estuary where flow convergence results in the concentration of particulate matter; this [process] usually operates through the interaction of particle (or organism) sinking and net-landward flow at depth," much of the literature is remarkably vague on exactly what the entrapment zone is. In general, however, it seems to be a catchall term that has been used synonymously with, and seems to encompass the terms such as turbidity maxima, biological maxima, null zone, and low salinity zone (or X2). Unlike the term entrapment zone, these other terms have precise definitions that are well documented in the literature. These terms are

not synonymous, even though they describe related phenomena. For example, the null zone has nothing to do with elevated concentrations of suspended sediment (or elevated concentrations of anything else). The null zone is simply the area where net landward flow near the bottom ceases and just downstream of where net flow throughout the water column is seaward (Figure 2-1).

An important element of the gravitational-circulation-based conceptual model of accumulation (Figure 2-1) is that the phenomena described by these related terms are co-located. *An* overarching term that generally describes a zone where all of these terms apply is useful if these things are actually occurring at the same place and time. On the basis of the analysis of the data described in this chapter, the null zone, turbidity and biological maxima and X2 can often occur at entirely different locations in the estuary. Therefore, if the primary utility of the term, entrapment zone, was to describe a region where these related phenomena were occurring simultaneously, then the term is misleading. Analysis of these data suggests that these related phenomena are not occurring at the same place and time, at least with respect to the residual currents, turbidity maximum, and X2.

Timescales

Another reason for the ambiguity in the use of the term entrapment zone, and the difficulty in understanding the underlying mechanisms that may create it, is the pervasive mixing of timescales in papers in which the entrapment zone is discussed. For example, from the Kimmerer (1993) definition of the entrapment zone, one could infer that the entrapment zone primarily evolves from the net landward flow at depth. It follows that if the entrapment zone evolves from a residual process such as the net currents determined through time averaging, then the entrapment zone itself is realizable only in a time-mean sense. Therefore, if the entrapment zone is defined in this way, the location of the entrapment zone cannot be determined from a single cruise, but from several cruises taken throughout a complete tidal cycle to be consistent with this definition.

Furthermore, Kimmerer (1993) defines the operational definition of the entrapment zone as having a surface salinity range of 1 to 6 psu without specifying the timescale. To be consistent with a gravitational circulation conceptual model of entrapment, the operational definition of the entrapment zone should be the position of the time-mean salinity range of 1 to 6 psu. In this chapter, an operational definition of the entrapment zone was used that follows the movement of the salt field (Lagrangian) and is consistent with the Kimmerer (1993) definition. This definition is consistent with the timescale of cruise data that form the basis of most of the entrapment zone literature to date, but is inconsistent with the Eulerian-based conceptual model of gravitational circulation and the null zone because the residual timescale is used in this conceptual model.

Given the confusion over the term entrapment zone some key terms used in this chapter are defined in a glossary of terms given at the end of this chapter.

Existing Conceptual Model of Entrapment in the North Bay

The generally accepted conceptual model of the entrapment zone is of an area in the estuary where a flow convergence results in an increased concentration of particulate matter through the interaction of particle (or organism) aggregation and sinking and net landward flow at depth (Arthur and Ball 1979; Kimmerer 1993). For this chapter, the terms, net, tidally averaged, and residual, imply timescales whose periods are significantly longer than the diurnal tidal period of about 25 hours. The null zone, which generally is believed to coincide with the landward limit of the entrapment zone, is a location in the estuary just landward of the cessation of residual landward flow near the bottom (Figure 2-1). The entrapment zone and null zone have been associated with the low salinity zone (salinity of 1 to 6 psu, Arthur and Ball 1979; Kimmerer 1993) and more recently associated with X2, the position of the near-bed, 2 isohaline (Jassby and others 1995). This model of the entrapment zone assumes the presence of gravitational circulation, a landward residual flow along the bottom of the estuary seaward of the low salinity zone.

Gravitational Circulation

The physics of gravitational circulation have been understood for at least four decades (Pritchard 1952; Postma and Kalle 1955) and have been well documented (Hansen and Rattray 1965; Peterson and others 1975; Officer 1976). For this chapter, gravitational circulation is a residual (tidally averaged), two-layer flow in which low-salinity water flows seaward in the surface layer, whereas denser, more saline water flows landward in the bottom layer. This two-layer flow results from the balance between the free surface slope acting in a down-estuary direction, and the longitudinal density (salinity) gradient acting in the landward direction (Officer 1976). See the appendix for the details of barotropic (free surface slope) and baroclinic (longitudinal density gradient) flows.

Principal Findings

Many of the principal findings in this report evolve directly from interpretations of the residual currents measured at fixed sites along the axis of north bay. Although the interaction of the tides and tidal currents with the residual currents are inherently nonlinear, the instantaneous current at any point in the estuary can be thought of as the sum of the currents from several independent processes (Figure 2-3). Except for the tidal currents, all the currents depicted in Figure 2-3 evolve from residual processes, which are at least an order of magnitude smaller than the tidal currents.

In this chapter we are primarily interested in the gravitational circulation component of the residual currents (Figure 2-3a) because gravitational circulation forms the basis of the historical conceptual model of entrapment in the north bay. In the following paragraphs, however, we place gravitational circulation in the context of the many other physical factors that can contribute to the residual currents. In practice, it is difficult, if not impossible, to separate out the individual contributions to the measured residual currents from the various mechanisms shown in Figure 2-3.

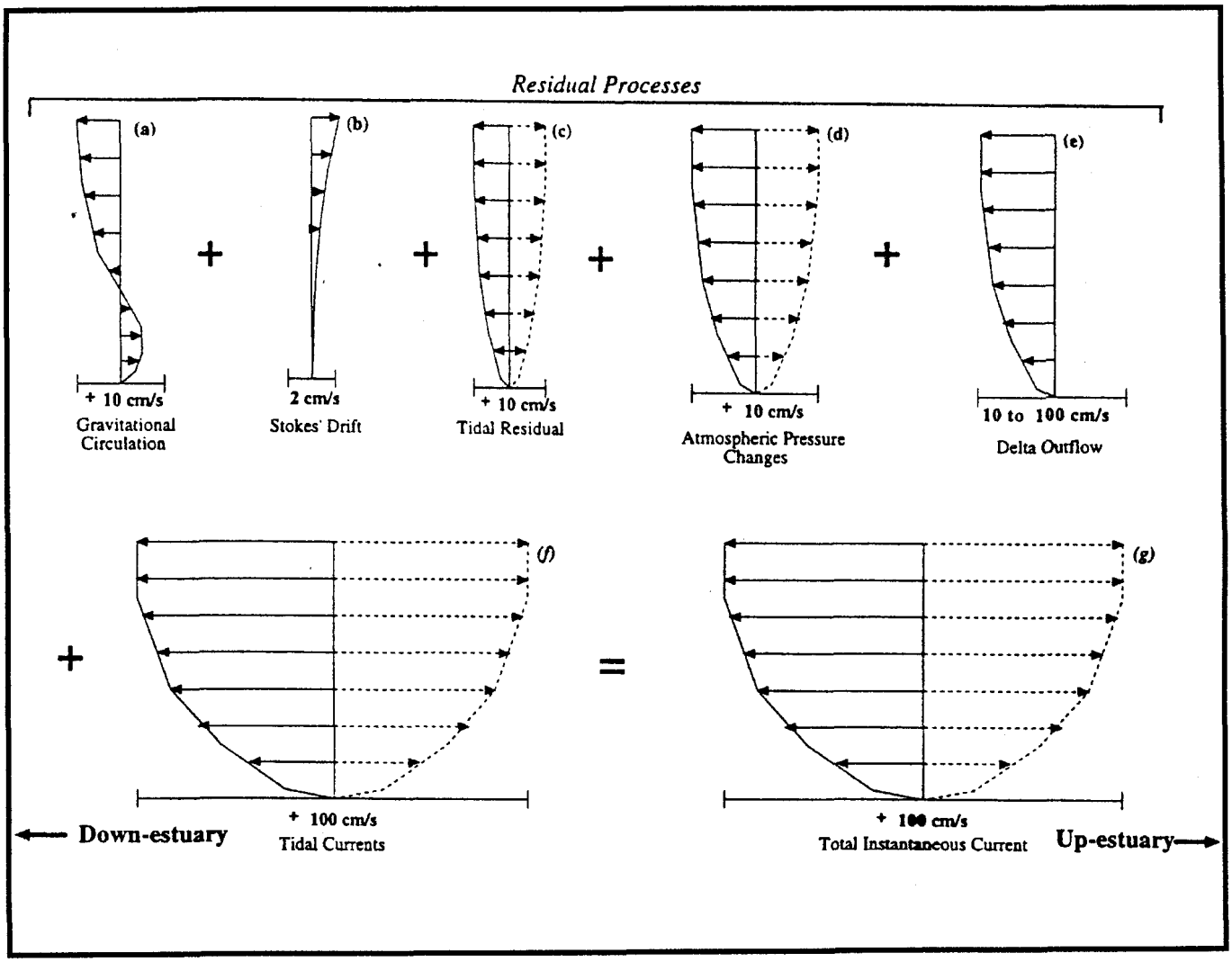

Figure 3
CONCEPTUAL MODEL OF THE TIDAL AND RESIDUAL CURRENTS IN THE NORTH BAY

Current magnitudes are approximate and vary considerably in time and space.

Dashed profiles in the landward direction are indicative of a process that can operate in either direction. The magnitudes of the tidal and residual currents given in this figure are order of magnitude estimates. Many of these values can vary, depending on location and season. The tidal residual evolves from the interaction of the tides with the bathymetry. (x = <x> + x', where <x> is a residual and x' is a deviation from the residual.) Current speed is shown in centimeters per second (cm/s).

However, in the final analysis, if the baroclinic pressure gradients are unable to create a net upstream residual current, we say that gravitational circulation is weak or nonexistent because without a net upstream residual current, entrapment from gravitational circulation is impossible, as defined.

The low-pass-filtered, or residual, velocities presented in this chapter represent the net result of all the residual processes depicted in Figure 2-3. So when the net near-bed currents are pointing in a landward direction on a low-pass-filtered stick (velocity) plot, we state that "no gravitational circulation was observed." What we really mean is that the sum total of the residual processes at a given location was such that the net near-bed currents were down-estuary (for example, gravitational circulation was weak relative to the other residual processes). A horizontal density gradient ($\frac{\partial \rho}{\partial x}$, where ρ is the velocity and x is the along-channel distance) driven flow (Figure 2-3a) may actually exist, but may

be overshadowed by the other residual processes, such as a barotropic mean flow (for example, delta outflow). Gravitational circulation is the only residual process that depends on the gradients in the density field.

Stokes' drift depends on the correlation between tidal timescale .water surface fluctuations (the tides) ′(ζ) and the tidal current, ***u'***, which creates a convex-shaped Eulerian residual profile that is landward directed (Figure 2-3b) (Najarian and others 1984). Tidal residuals are generated through the interaction of the tides and tidal currents with the basin bathyrnetry (Figure 2-3c). Atmospheric pressure changes can induce exchanges between the Pacific Ocean and the entire San Francisco Bay system (Figure 2-3d). The water level in the delta can be raised as much as 0.4 m by a large atmospheric pressure drop. Delta outflow introduces a residual current throughout the north bay that varies with the amount and timing of the outflow. Residual currents, on the order of the tidal currents [~ 1 meter per second (m/s)], caused by delta outflow, can occur in the channels during large, uncontrolled winter flows (Figure 2-3e).

Three of the residual processes shown in Figure 2-3 have fortnightly (spring/neap) components. Gravitational circulation varies with the intensity of the vertical mixing; during spring tides, vertical mixing is strong and gravitational circulation, if it exists, is weaker. Because the tide-induced residual involves nonlinear interaction between the tides, tidal currents, and the basin bathymetry, it is expected that spring tides enhance this interaction (Walters and others 1985). The same is true for Stokes' drift; greater tidal range and tidal-current magnitudes during spring tides increase the magnitude of their correlation.

Except for gravitational circulation and Stokes' drift, the remaining residual processes are forced by water-surface slopes, which essentially yield a characteristic log profile, as shown in Figure 2-3. Barotropic pressure gradients in the presence of strong vertical stratification can yield nonlog profiles; however, these nonlinear interactions are beyond the scope of this chapter. Even though these interactions may be important in creating ebb/flood asymmetries in near-bed shear and vertical mixing that could contribute to concentration maxima in regions in the bay where gravitational circulation is weak, the study of these interactions is in its infancy and a topic of active research.

Because the position of the salt field and the strength of its gradients depend primarily on the uncontrolled winter freshwater flows into Suisun Bay, the timing and strength of gravitational circulation depend primarily on the hydrology in a given year. During 1994, a fairly dry year when peak delta outflows were less than 1,000 cubic meters per second (m3/sec) (Figure 2-4), the salt field was relatively far landward and X2 was near, or landward of, Mallard Island. Mallard Island has a river kilometer index (RKI) of 75 kilometers (km).

Gravitational Circulation

Approximate locations of the ADCPs deployed during the 1994 entrapment zone study are shown in Figure 2-2. ADCPs measure the velocity at a sequence of evenly spaced intervals above the bed. These measurement locations are referred to as "BINs" where BIN 1 is the velocity measurement nearest to the bottom. Data collected from ADCPs deployed in the southern channel of Suisun Bay (stations: CONC, CNCRD, MAL) and the western delta (stations: ANTCH, MK8) indicate little evidence of gravitational circulation, even though the mean position of the near-bed 2 isohaline was near or landward of Mallard Island (Figure 2-5). Specifically, ADCP data collected near Concord (Figure 2-6) and Mallard Island (Figure 2-7) indicate

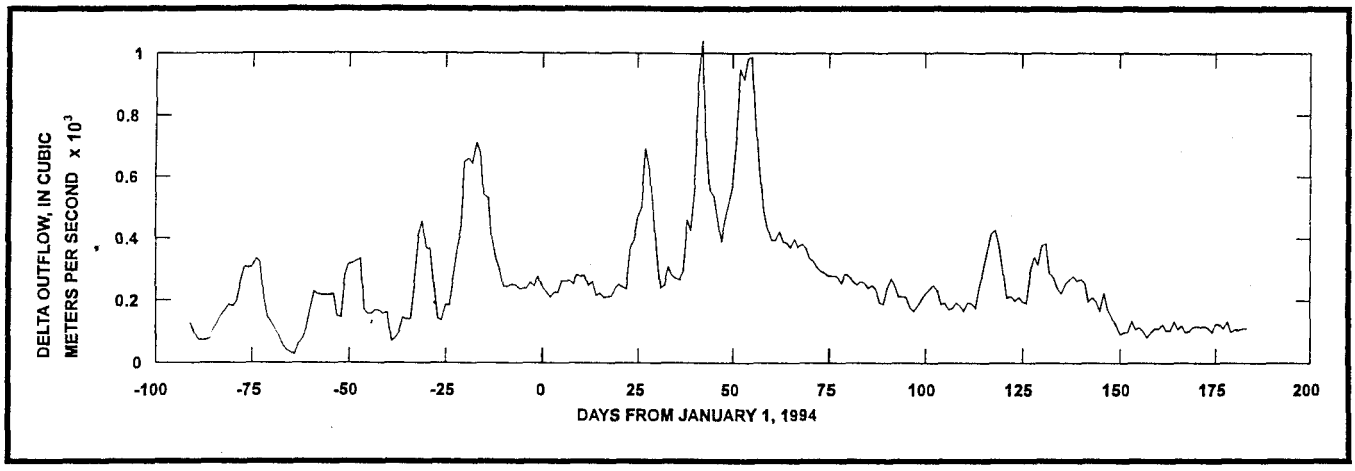

Figure 4
DELTA OUTFLOW ESTIMATES (DAYFLOW), OCTOBER 1, 1993, TO JULY 1, 1994, SUISUN BAY

near-bed residual currents that were directed seaward, indicating a lack of, or relatively weak, gravitational circulation. In contrast, the ADCP data collected in Carquinez Strait near Martinez (station MRTNZ) from April 22 to June 15, 1994, show strong residual near-bed currents of 15 to 20 cm/s directed landward (Figure 2-8). ADCP data collected by NOAA in Carquinez Strait (Figure 2-9) and near Concord (Figure 2-10) from April 22 to May 22, 1992, are consistent with the data collected in 1994 in that near-bed residual currents in Carquinez Strait were landward, and near-bed residual currents were seaward at Concord, even though these data were collected during different water year types. During the 1992 NOAA deployments, X2 was also landward of Mallard Island.

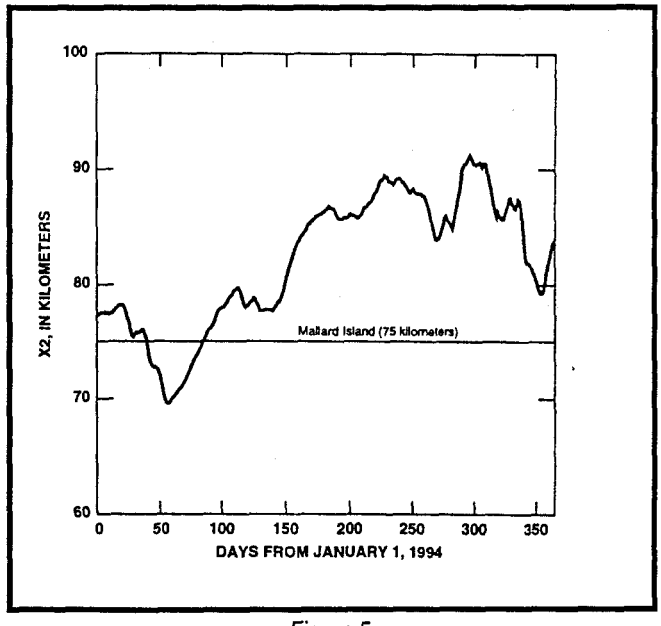

Figure 5
X2 COMPUTED FROM AN ARIMA MODEL THAT PREDICTS X2 FROM LOG DELTA OUTFLOW AND YESTERDAY'S X2 (Jassby and others 1995)
X2 is the along-channel distance from the Golden Gate of the near-bed salinity of 2 psu. (KM=kilometers.).

The observed magnitude of landward near-bed residual currents in the Carquinez Strait ADCP (CAR in Figure 2-2) data, coupled with the seaward near-bed residual currents in the southern channel of Suisun Bay, indicates the possibility of a topographic control of the gravitational circulation at the Benicia Bridge (Figure 2-2) where the depths change from about 19 m in Carquinez Strait to about 11 m in Suisun Bay. The concept of topographic control is well known (Armi 1986; Farmer and Armi 1986). The large decrease in depth, coupled with a large decrease in width just landward of the Benicia Bridge, likely is responsible for the reduction in near-bed residual currents from 15 to 20 cm/s landward in Carquinez Strait to 5 to 10 cm/s seaward at Concord (CNCRD in Figure 2-2) in the 1992 and the 1994 data sets. A null zone (area where the near-bed residual current changes from landward to seaward) was geographically fixed to an area near the Benicia Bridge during spring

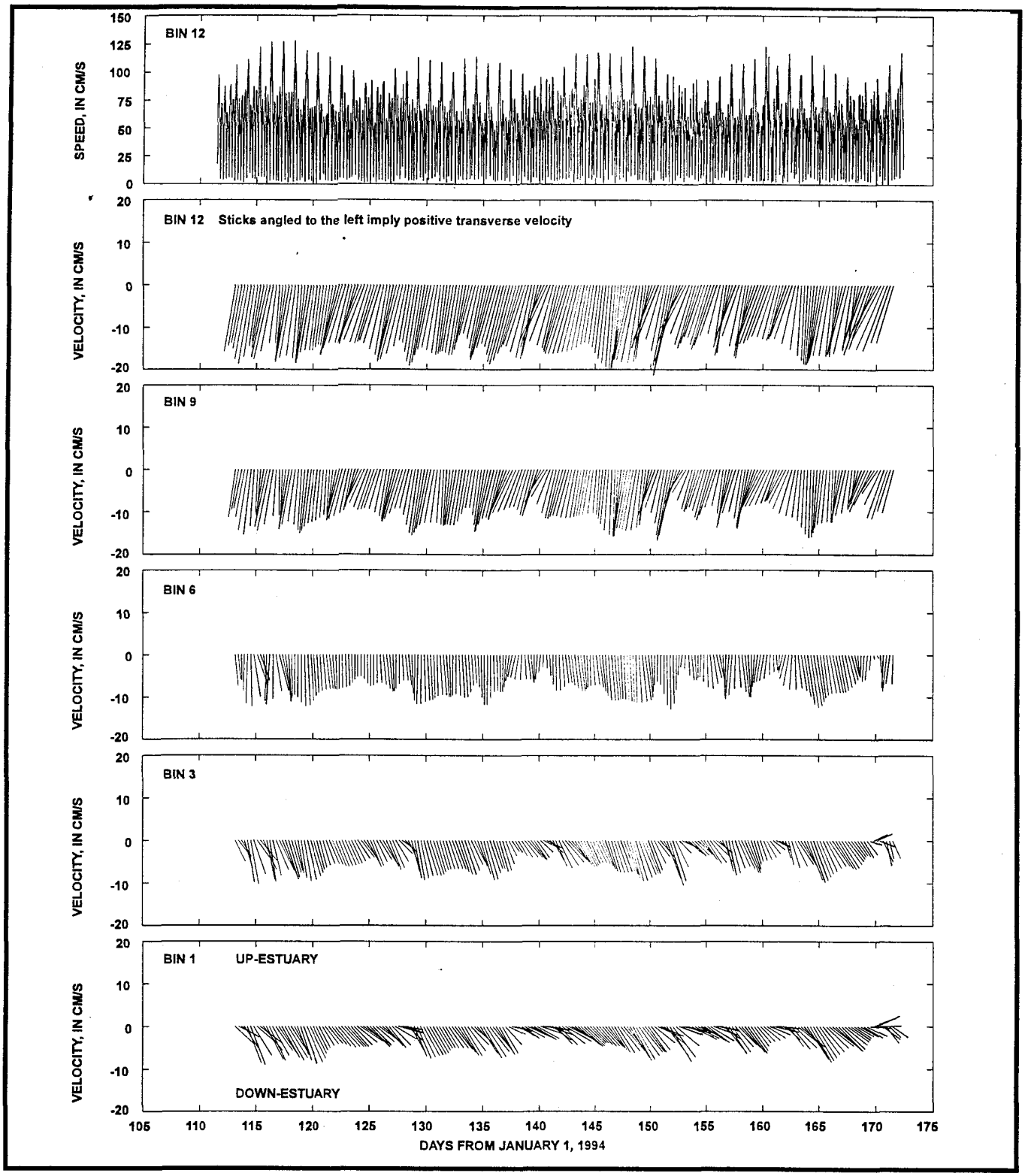

Figure 6
STICK PLOTS OF RESIDUAL CURRENTS AT STATION CNCRD (near Concord),
APRIL 4 THROUGH JUNE 21, 1994, SUISUN BAY

Tidal current speed at velocity measurement location (BIN) 12 is shown in the top panel for reference.
The velocity measurement at BIN 1 is located 1.9 meters off the bed. The remaining BINS are evenly spaced toward the surface at 1-meter intervals (for example, BIN 2 is at 2.9 meters, etc.). Principal direction is 82.0 degrees relative to true north. Velocity and speed are given in centimeters per second (cm/s).

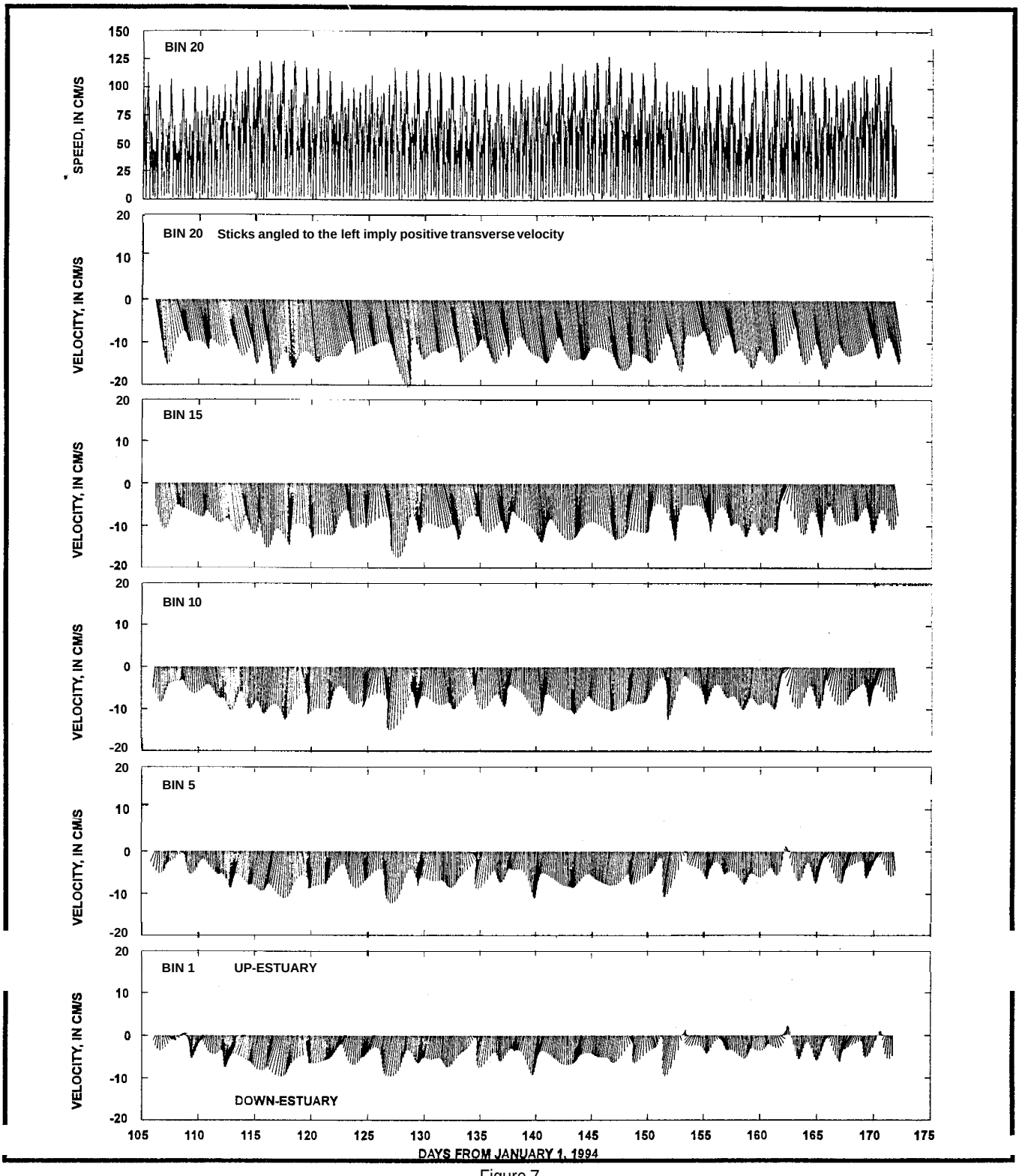

Figure 7
STICK PLOTS OF RESIDUAL CURRENTS AT STATION MAL (near Mallard Island),
APRIL 14 THROUGH JUNE 20,1994, SUISUN BAY

Tidal current speed at velocity measurement location (BIN) 20 is shown in the top panel for reference.
The velocity measurement at BIN 1 is located 1.9 meters off the bed. The remaining BINS are evenly spaced toward the surface at 0.5-meter intervals (for example, BIN 2 is at 2.4 meters, etc.). Principal direction is 107.0 degrees releative to true north.
Velocity and speed are given in centimeters per second (cm/s).

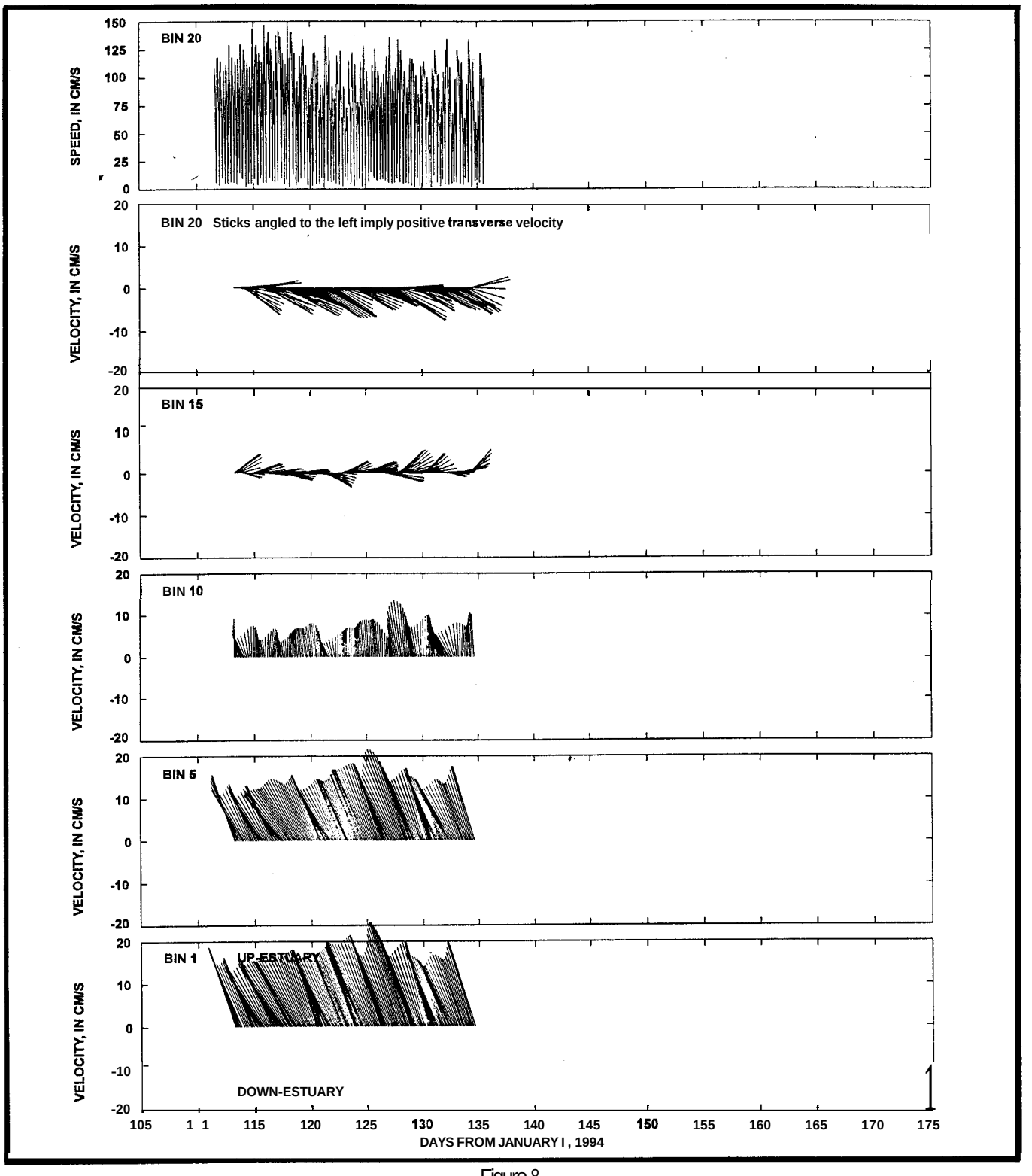

Figure 8
STICK PLOTS OF RESIDUAL CURRENTS AT STATION MRTNZ (near Martinez),
APRIL 21 THROUGH JUNE 22,1994, MARTINEZ

Tidal current speed at velocity measurement location (BIN) 20 is shown in the top panel for reference.
The velocity measurement at BIN 1 is located 1.9 meters off the bed. The remaining BINS are evenly spaced toward the surface at 0.5-meter intervals (for example, BIN 2 is at 2.4 meters, etc.) Principal direction is 75.0 degrees relative to true north.
Velocity and speed are given in centimeters per second (cm/s).

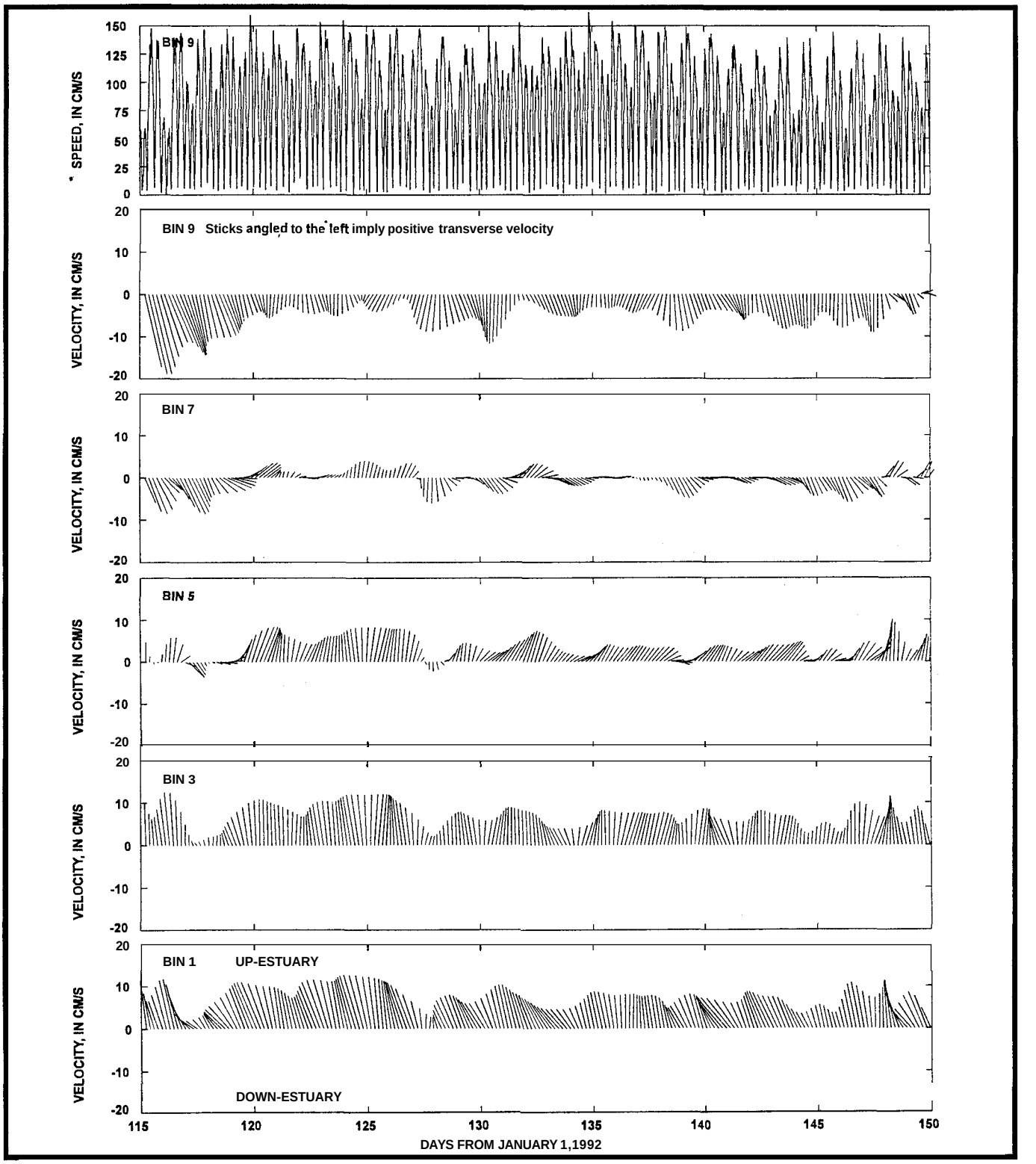

Figure 9
STICK PLOTS OF RESIDUAL CURRENTS AT STATION CAR (in Carquinez Strait),
APRIL 23 THROUGH MAY 30,1992, CARQUINEZ STRAIT

Tidal current at velocity measurement location (BIN) 9 is shown in the top panel for reference.
The velocity measurement at BIN 1 is located 1.9 meters off the bed. The remaining BINS are evenly spaced toward the surface at 1-meter intervals (for example, BIN 2 is at 2.9 meters, etc.). Principal direction is 91.0 degrees relative to true north.
Velocity and speed are given in centimeters per second (cm/s).

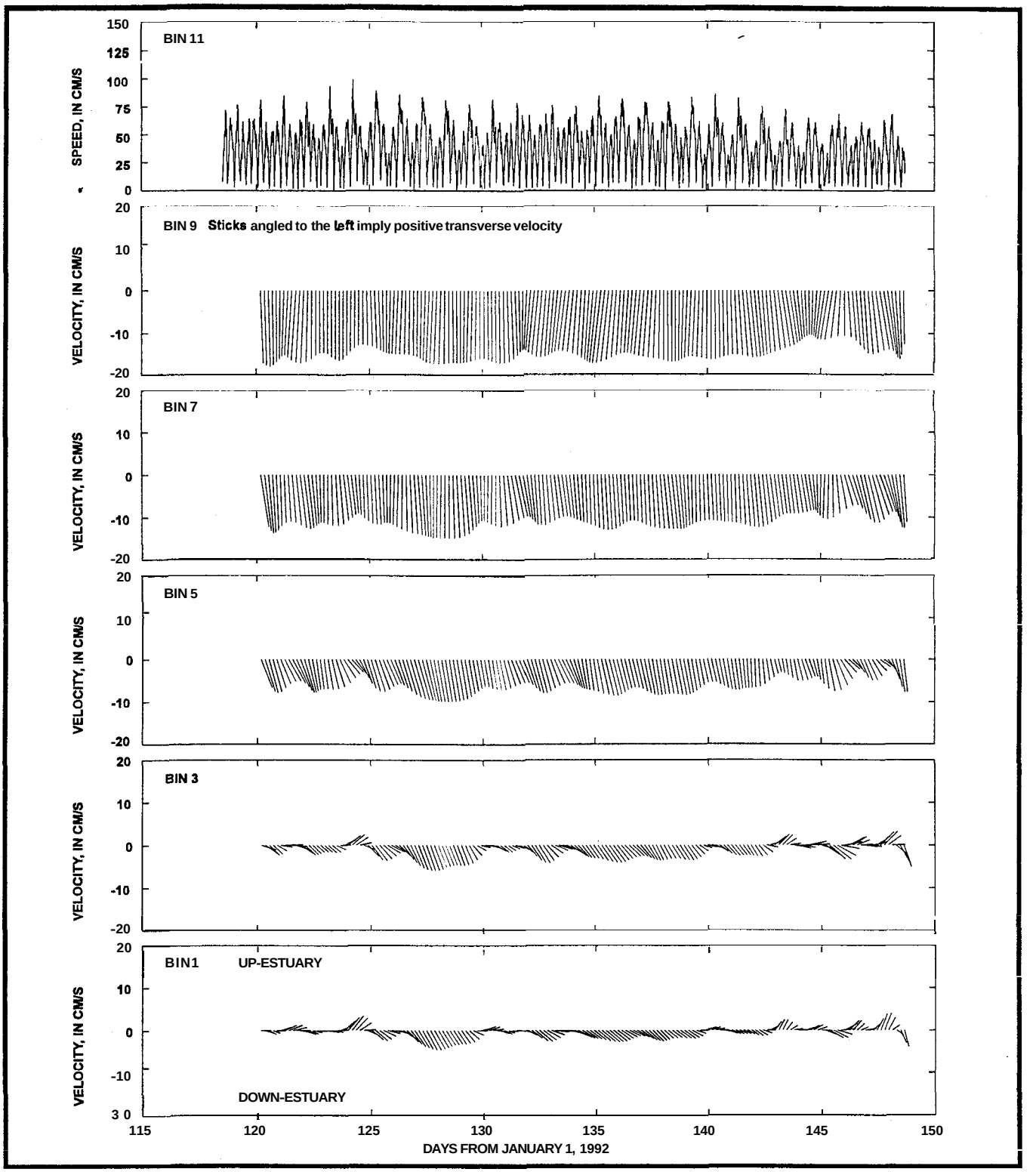

Figure 10
STICK PLOTS OF RESIDUAL CURRENTS AT STATION CONC (near Concord Naval Weapons Station), APRIL 28 THROUGH MAY 29,1992, SUISUN BAY

Tidal current speed at velocity measurement location (BIN) 11 is shown in the top panel for reference.
The velocity measurement at BIN 1 is located 1.9 meters off the bed. The remaining BINS are evenly spaced toward the surface at 1-meter intervals (for example, BIN 2 is at 2.9 meters, etc.). Principal direction is 91.0 degrees relative to true north.
Velocity and speed are given in centimeters per second (cm/s).

1992 and spring 1994, even though the mean position of the 2-psu near-bed isohaline was near or landward of Mallard Island during these time periods. These data conflict directly with the idea that a null zone is located near X2. Moreover, other data indicate that vertical constrictions of the channels (Pinole Shoal, for example; Figure 2-2) can create local null zones (Walters and Gartner 1985). These results suggest the possibility of several distinct gravitational circulation cells in the north bay separated by sills in the channels.

Delta Acoustic Doppler Current Profiler Data

As part of the 1994 entrapment zone study, two ADCPs were deployed in the delta (ANTCH and MK8, Figure 2-2). Residual currents in the Sacramento River at channel marker 8 and the San Joaquin River near Antioch are shown in Figures 2-11 and 2-12, respectively. Although these data show weak landward residual currents (<5 cm/s) near the estuary bed, they do not indicate the presence of gravitational circulation because a dynamically significant horizontal salinity gradient was absent (for example, time-mean salinities in excess of 2 psu). Such a gradient was not present at either of these locations during the 1994 study (Figures 2-13 and 2-14). The near-bed landward flows observed in the MK8 data near day 115 and day 150 (Figure 2-11) likely were caused by atmospheric pressure drops that occurred during these times (Figure 2-15). Atmospheric-pressure-induced residual velocities are distinguishable (1) from gravitational circulation because atmospheric pressure changes affect the entire water column (barotropically-driven log profile), and (2) from delta outflow because of the relatively short duration of atmospheric pressure-change induced residuals relative to delta outflow induced residuals.

The residual current profiles observed in the delta (Figures 2-11 and 2-12) exhibit a greater shear than would be expected from a pure barotropic flow. Two possible explanations for this are: (1) lateral ebb/flood current asymmetries could exist at both stations because both stations were located relatively close to channel bends, and (2) tidal timescale baroclinicity occurred near high water slack tide. The first explanation also could account for the residual surface current flowing at right angles to the channel.

Atmospheric pressure changes appear to produce a greater response at the San Joaquin River station then at the Sacramento River station. Atmospheric pressure-related net upstream currents can be seen near days 115, 135, 150, and 160 in the Antioch data (Figure 2-12), whereas the Sacramento River data indicate little or no response (Figure 2-11). A likely explanation for the apparent greater atmospheric coupling on the San Joaquin River is the greater surface area on the San Joaquin side of the delta. Because of the relatively small size of San Francisco Bay [1.04×10^9 square meters (m^2)], Conomos 1979) compared with the spatial scale of atmospheric pressure fluctuations (Walter and Gartner 1985), water-level changes that occur in this system are driven by exchanges with the Pacific Ocean, which means that water levels throughout the bay and delta rise and fall approximately coherently (for example, without spatial gradients) with changes in atmospheric pressure. Therefore, if the delta rises approximately uniformly, then the volume of water that must flow through a given delta channel depends entirely on its upstream surface area. Because the San Joaquin River has the greater surface area, the currents there have a greater response to atmospheric pressure fluctuations.

Wind has a significant effect on the circulation in lakes and in estuaries. For

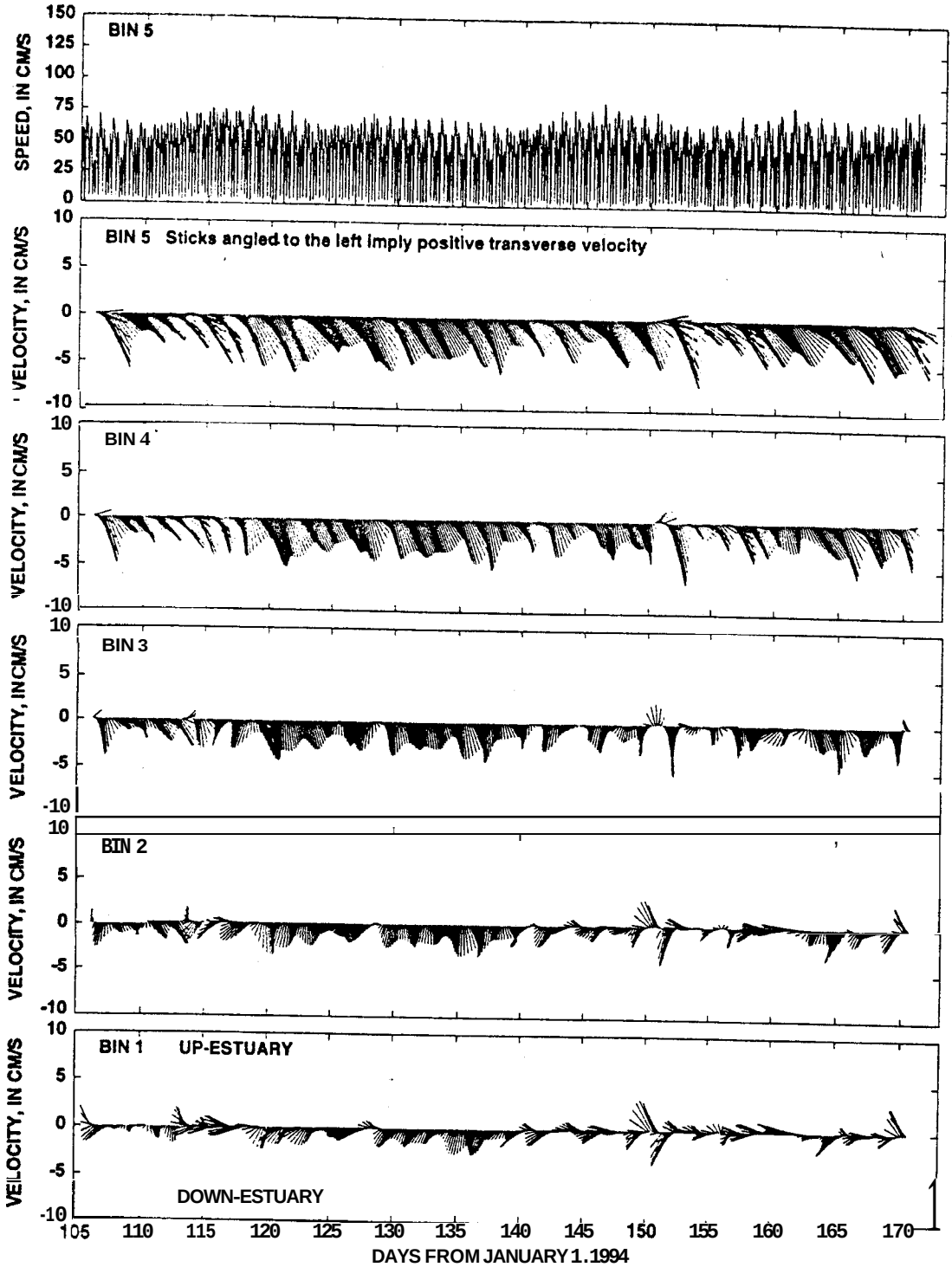

Figure 11
STICK PLOTS OF RESIDUAL CURRENTS AT STATION MK8 (Sacramento River near channel marker 8), APRIL 14 THROUGH JUNE 20,1994, SACRAMENTO RIVER

Tidal current speed at velocity measurement location (BIN) 5 is shown in the top panel for reference.

The velocity measurement at BIN 1 is located 1.9 meters off the bed. The remaining BINS are evenly spaced toward the surface at I-meter intervals for example, BIN 2 is at 2.9 meters, etc.). Principal direction is 99.0 degrees relative to true north.

Velocity and speed are given in centimeters per second (cm/s).

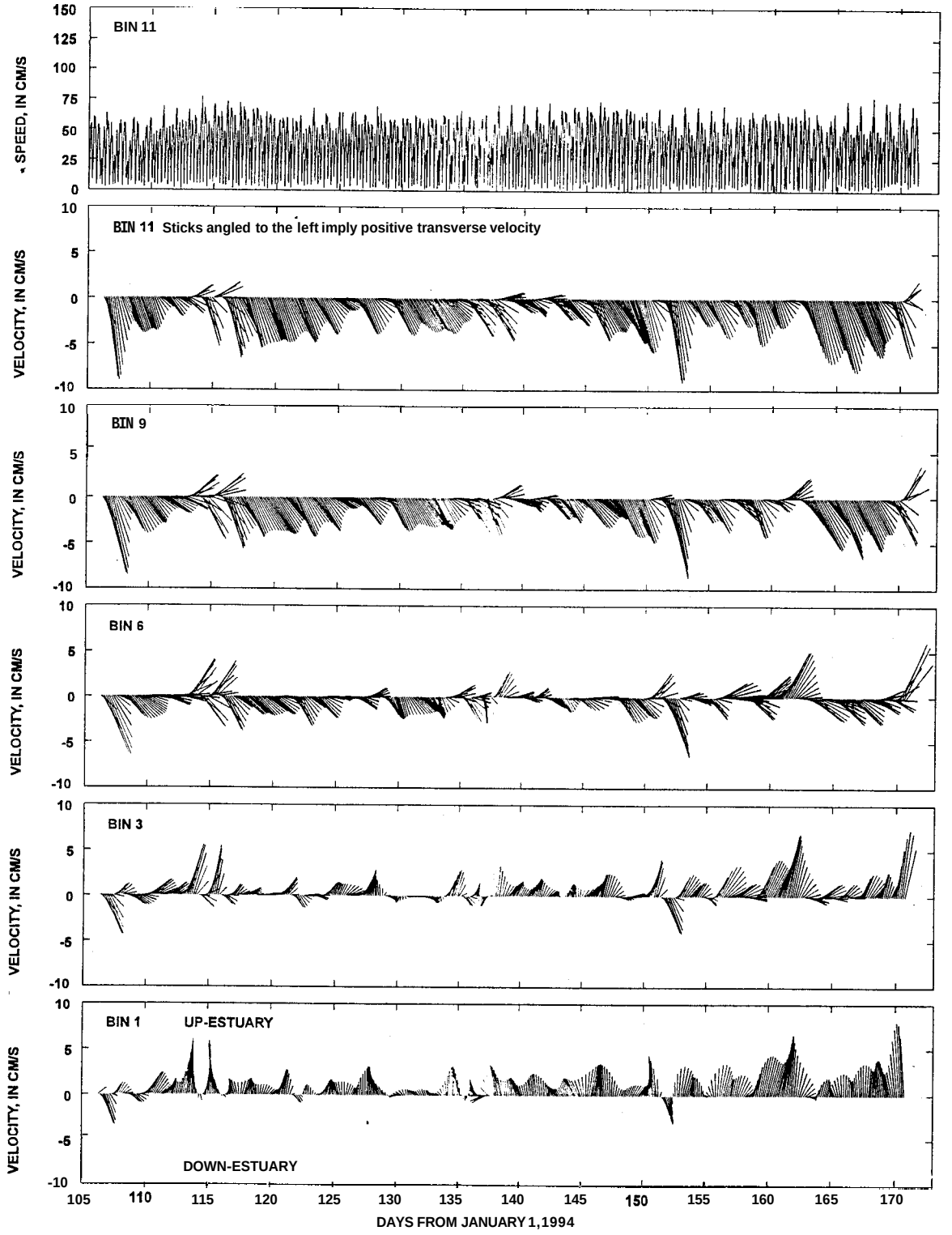

Figure 12

STICK PLOTS OF RESIDUAL CURRENTS AT STATION ANTCH (near Antioch), APRIL 14 THROUGH JULY 20,1994, ANTIOCH

Current speed at velocity measurement location (BIN) 11 as shown in the top panel for reference.

The velocity measurement at BIN 1 is located 1.9 meters off the bed. The remaining BINS are evenly spaced toward the surface at 1-meter intervals (for example, BIN 2 is at 2.9 meters, etc.). Principal direction is 109.0 degrees relative to true north.

Velocity and speed are given in centimeters per second (cm/s).

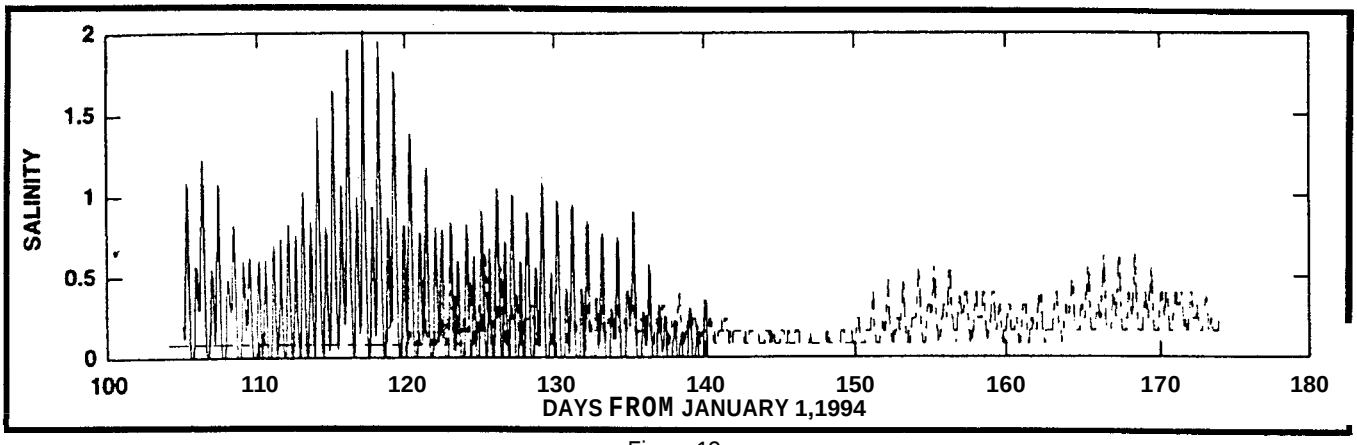

Figure 13
TIME SERIES PLOT OF NEAR-BED (solid) AND NEAR-SURFACE (dashed) SALINITY AT ANTIOCH

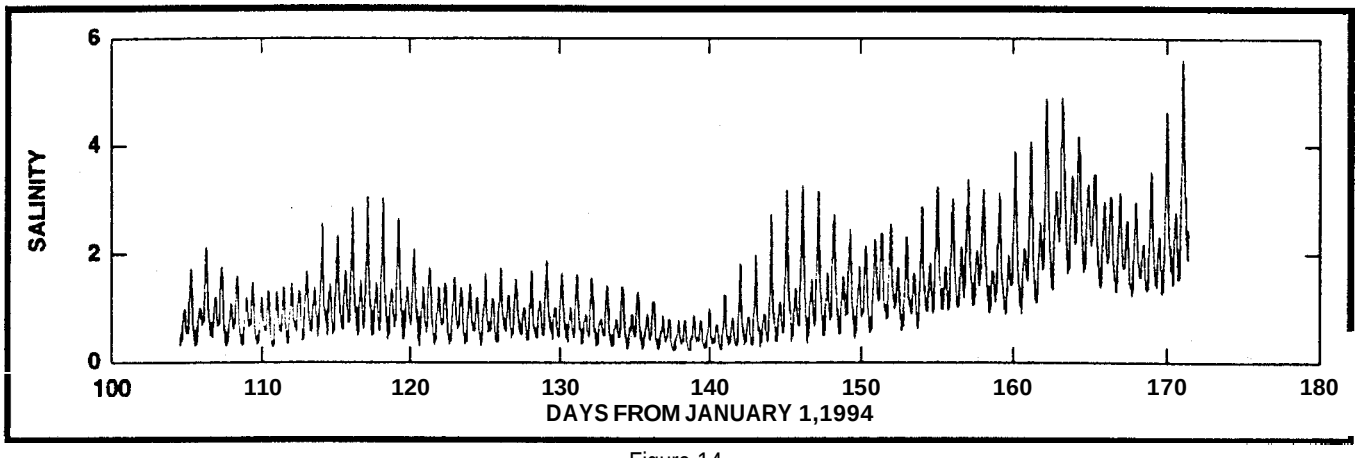

Figure 14
TIME SERIES PLOT OF NEAR-BED SALINITY ON THE SACRAMENTO RIVER AT CHANNEL MARKER 8, SACRAMENTO RIVER

example, many micro-tidal estuaries are almost completely wind driven. In San Francisco Bay, however, no correlation between the wind and the residual currents for summer conditions has been observed in the north bay (Walters and Gartner 1985). Also, periods of large persistent winds in San Francisco Bay usually are caused by significant atmospheric pressure changes, making it difficult to separate the effects of wind from the effects of atmospheric pressure. Although Warner and others (1997) found a correlation between the wind and residual currents at a single location in Honker Bay, current/wind correlations need to be done on the more recently collected hydrodynamic data.

In summary, analysis of the data described in this chapter and a review of all historical near-bed current-meter data collected in Suisun Bay (Peterson and others 1975; Cheng and Gartner 1984; Walters and Gartner 1985; Mortenson 1987; Monismith and others 1996) and in the Sacramento River (Nichol 1996) indicate the following spatial and temporal characteristics of gravitational circulation in the north bay of San Francisco Bay:

1. Gravitational circulation dominates residual currents in Carquinez Strait unless freshwater inflows are so high that the waters in Carquinez Strait are completely fresh. Recently collected indirect evidence (decreased stratification and suspended-sediment concentrations in the autumn at the Benicia Bridge) sug-

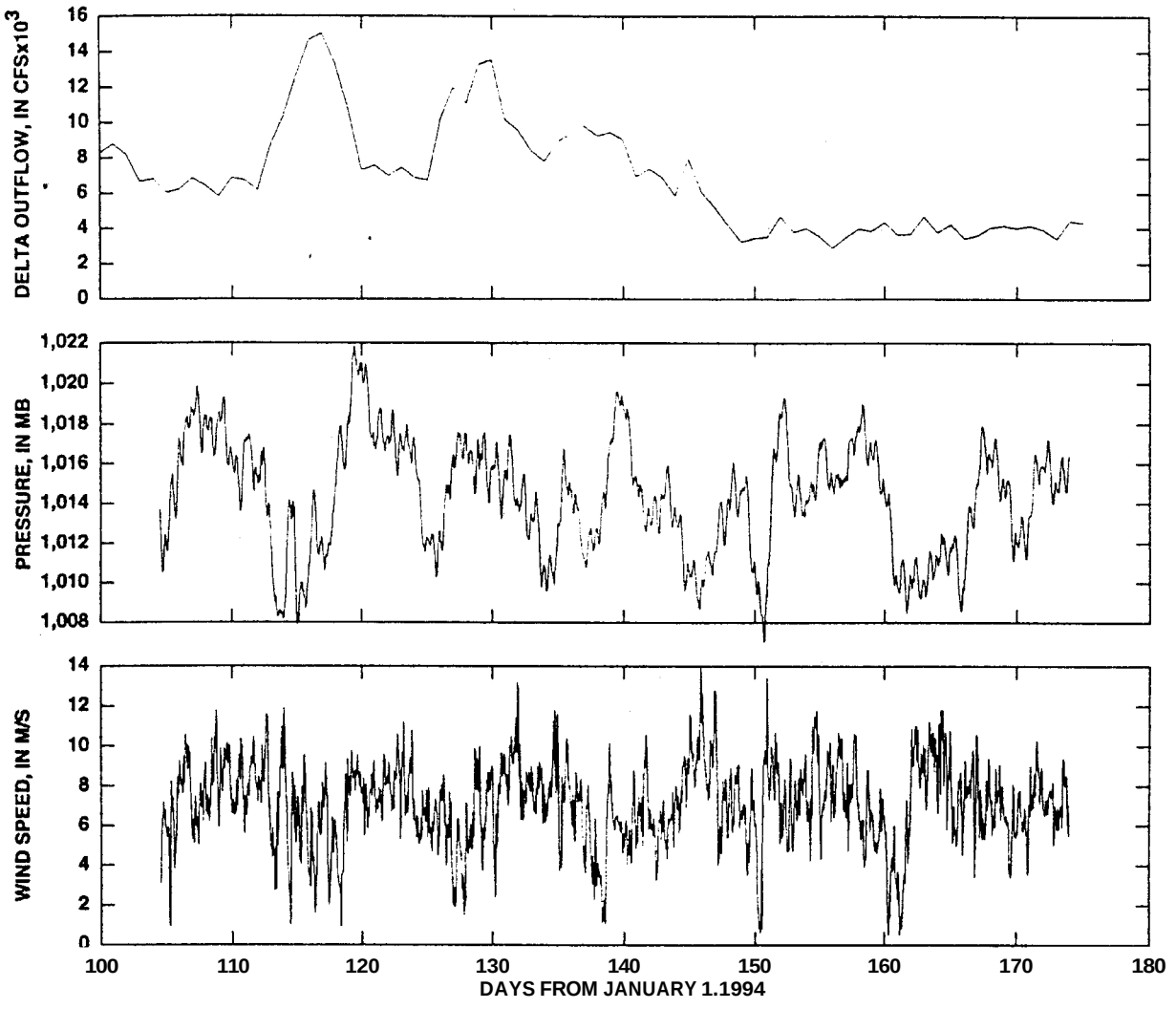

Figure 15
DELTA OUTFLOW INDEX (DAYFLOW) (top), ATMOSPHERIC PRESSURE (middle), AND WIND SPEED (bottom) AT CHANNEL MARKER 27 IN SUISUN BAY
Winds during this period generally were from the east. Direction is about 270 degrees.
(M/S=meters per second; MB=millibar; CFS=cubic feet per second.)

gests that gravitational circulation de-creases in the autumn as the horizontal salinity gradient moves landward of Carquinez Strait.

Gravitational circulation is rare in Suisun Bay during the spring, but has been consistently measured during the autumn in the northern part of Suisun Bay (Walters and Gartner 1985; Mortenson 1987; Stacey 1996).

3. Gravitational circulation has been measured in the Sacramento River at channel marker 14 (not shown in Figure 2-2) when local near-bed salinities have exceeded about 2 psu (Nichol 1996).

4. When gravitational circulation is present in the north bay, its magnitude is modulated by the fortnightly (14-day period) spring/neap cycle. Gravitational circulation is weakest during spring tides and strongest during neap tides (Burau and others 1993).

The available data indicate a seasonal variability in the strength of the gravitational circulation in the eastern portion of Suisun Bay, which is tied through the salt field (horizontal density gradient) to winter freshwater flows that control the location and strength of the horizontal salinity gradient. Throughout most of the year, gravitational circulation appears .to be weak or absent in the ship channel in Suisun Bay. Gravitational circulation is not likely to be the principal mechanism responsible for accumulation of particles and organisms in the low salinity zone (−2 psu) when this zone is located in the ship channel of Suisun Bay. In the following sections, a revised conceptual model based on scaling arguments (stratification timescale) is discussed that demonstrates how gravitational circulation works in Suisun Bay and at least qualitatively explains the depth, fortnightly, and seasonal variability observed. Finally, alternate entrapment mechanisms are discussed.

Revised Conceptual Model of Entrapment

In the following section, a conceptual model is presented that predicts the rarity of gravitational circulation in the southern channel of Suisun Bay, but predicts that gravitational circulation can occur in Suisun Cutoff and in the western delta during autumn.

Revised Conceptual Model of Gravitational Circulation

On the basis of one-dimensional (ID) modeling of stratified water columns, a nondimensional parameterization of gravitational circulation strength can be constructed (Monismith and others 1996) known as the horizontal Richardson number

$$Ri_x = \frac{g}{\rho_o}\frac{H^2}{U_s^2}\frac{\partial \rho}{\partial x} \qquad (1)$$

where g is gravitational acceleration, H is the mean depth, ρ is density and ρ_o is a reference density (freshwater) and "x" is a distance in the along-channel direction, and U_s is the near-surface velocity. A more intuitive form of equation 1 is

$$Ri_x = \frac{\left(\frac{g}{\rho_o}\right)\frac{\partial \rho}{\partial x}}{\left(\frac{U_s}{H}\right)^2}. \qquad (2)$$

In this form, Ri_x can be thought of as a balance (or ratio) between two competing mechanisms. The numerator contains the horizontal density gradient $\left(\frac{\partial \rho}{\partial x}\right)$ that drives the gravitational circulation, which also stratifies and thereby stabilizes the water column. The tendency of the horizontal density gradient to stratify the water column is balanced against the (water column average) vertical shear $\left(\frac{U_s}{H}\right)$ squared, which tends to break down the stratification through vertical mixing, ultimately reducing the strength of the gravitational circulation.

To reinforce the idea of the horizontal Richardson number representing the ratio of two competing processes, this nondimensional number can be thought of as the squared ratio of two timescales (Figure 2-16). The inverse of the horizontal Brunt-Vaisala frequency (Nunes Vaz and others 1989),

$$Ri_x = \frac{\tau_o^2}{\tau_s^2} = \frac{\frac{g}{\rho_o}\frac{\partial \rho}{\partial x}}{\left(\frac{U_s}{H}\right)^2}$$

Horizontal density difference drives gravitational circulation

Shear (mixes water column) Shuts down gravitational circulation

$$Ri_x = \frac{g H^2}{\rho_o U_s^2}\frac{\partial \rho}{\partial x} = \left(\frac{\tau_o}{\tau_s}\right)^2$$

$$\tau_s = \sqrt{\frac{\rho_o}{g\frac{\partial \rho}{\partial x}}}$$

Stratification Timescale

Exchange flow creates stratification

ρ_f

Δx

Δx

$$\tau_o = \frac{H}{U_s}$$

Overturning Timescale

Mixing breaks down stratification

U_s

ρ_f

Figure 16
HORIZONTAL RICHARDSON NUMBER: A RATIO OF TWO TIMESCALES

$$\tau_s = \sqrt{\frac{1}{\frac{g}{\rho_o}\frac{\partial \rho}{\partial x}}}, \quad (3)$$

represents what is referred to as the stratification timescale. This timescale, for example, represents the time it takes for two fluids of different densities separated by a wall to exchange after the wall is removed. The straining or overturning timescale,

$$\tau_o = \frac{H}{U_s}, \quad (4)$$

is a representative time for vertical mixing to break down stratification. The square of the ratio of the overturning timescale to the stratification timescale is the horizontal Richardson number given in equation 1,

$$Ri_x = \left(\frac{\tau_o}{\tau_s}\right)^2 \quad (5)$$

If the stratification timescale is short (stratification occurs rapidly—small τ_s) and vertical mixing is weak (overturns take a long time—large τ_o), the Richardson number will be large, indicating the possibility of gravitational circulation. Conversely, if τ_s is large and τ_o is small, gravitational circulation likely will not occur. An alternate interpretation is given by

Monismith and others (1996) and Stacey (1996).

Horizontal Richardson Number

The stratification timescale, τ_s, depends on the salt field, which in turn depends on delta outflow that varies from year-to-year, depending on hinter runoff. The overturning timescale, τ_o, on the other hand, is easy to estimate because the mean depth, H, and the near-surface (top meter) tidal current speed, U_s, can be easily measured and remain fairly constant.

Overturning or Straining Timescale

An estimate of the overturning timescale, based on the root-mean-square (RMS) surface current speed and the mean depth, as a function of the RKI, is plotted in Figure 2-17. Large values of τ_o (longer mixing timescale) have a greater probability of supporting a gravitational circulation cell for a given horizontal density gradient. Therefore, based on a horizontal Richardson number scaling, gravitational circulation is likely to occur (from left to right on Figure 2-17): (1) seaward of RKI 25, (2) in Carquinez Strait, **(3)** in the Reserve Fleet Channel, (4) in Suisun Cutoff, and (5) landward of Mallard Island.

Basically, gravitational circulation occurs seaward of RKI 25 and in Carquinez Strait because both are deep (relative to the strength of the tidal currents). Gravitational circulation occurs in the Reserve Fleet/Suisun Cutoff channel and landward of Mallard Island because the tidal currents are relatively weak in these locations. Friction (primarily) reduces the tidal current by about half across Suisun Bay, and the shallows **(–3** m) at both ends of Suisun Cutoff reduce the tidal currents. In contrast, locations on the overturning timescale plot, where the curve is low, are locations where gravitational circulation is not likely to occur (from left to right on Figure 2-17): (1) Pinole Shoal, (2) the ship channel in Suisun Bay (bounded by the Benicia Bridge to the west and Mallard Island to the east), and **(3)** the shallow areas to the northeast and southwest of Suisun Cutoff. Therefore, Pinole Shoal, the Benicia Bridge, and the shallow areas to the northeast and southwest of Suisun Cutoff are likely null zone locations when X2 is landward of these locations. The overturning timescale explains why gravitational circulation has been measured in Carquinez Strait, but is rarely observed in the shipping channel in Suisun Bay.

The overturning timescale also explains several apparently anomalous data sets. It explains, for example, why gravitational circulation was measured in Suisun Cutoff by Mortenson (1987) and by Stacey (1996). This timescale also explains why Nichol (1996) measured gravitational circulation at RKI 90 in the Sacramento River in 1987, 1989, and 1991-93 (all dry years when X2 was landward of this location).

Figure 2-17 shows that Carquinez Strait, Suisun Cutoff, and, interestingly, upstream of Mallard Island have a greater potential to produce a gravitational circulation cell for a given horizontal salinity gradient than does the ship channel in Suisun Bay where the overturning timescale is shorter. The weaker tidal currents in Suisun Cutoff and in the delta account for the long overturning timescales observed at these locations in the estuary. The tidal current magnitudes are reduced by roughly a factor of two between the west end of Carquinez Strait and Decker Island on the Sacramento River (bottom panel, Figure 2-17).

Moreover, sections of the Sacramento and San Joaquin rivers are deeper than the shipping channel in Suisun Bay, which adds to the potential for gravitational circulation in these locations. Figure 2-18 summarizes the basic residual current patterns that might be observed when X2 is landward of the confluence. Regardless

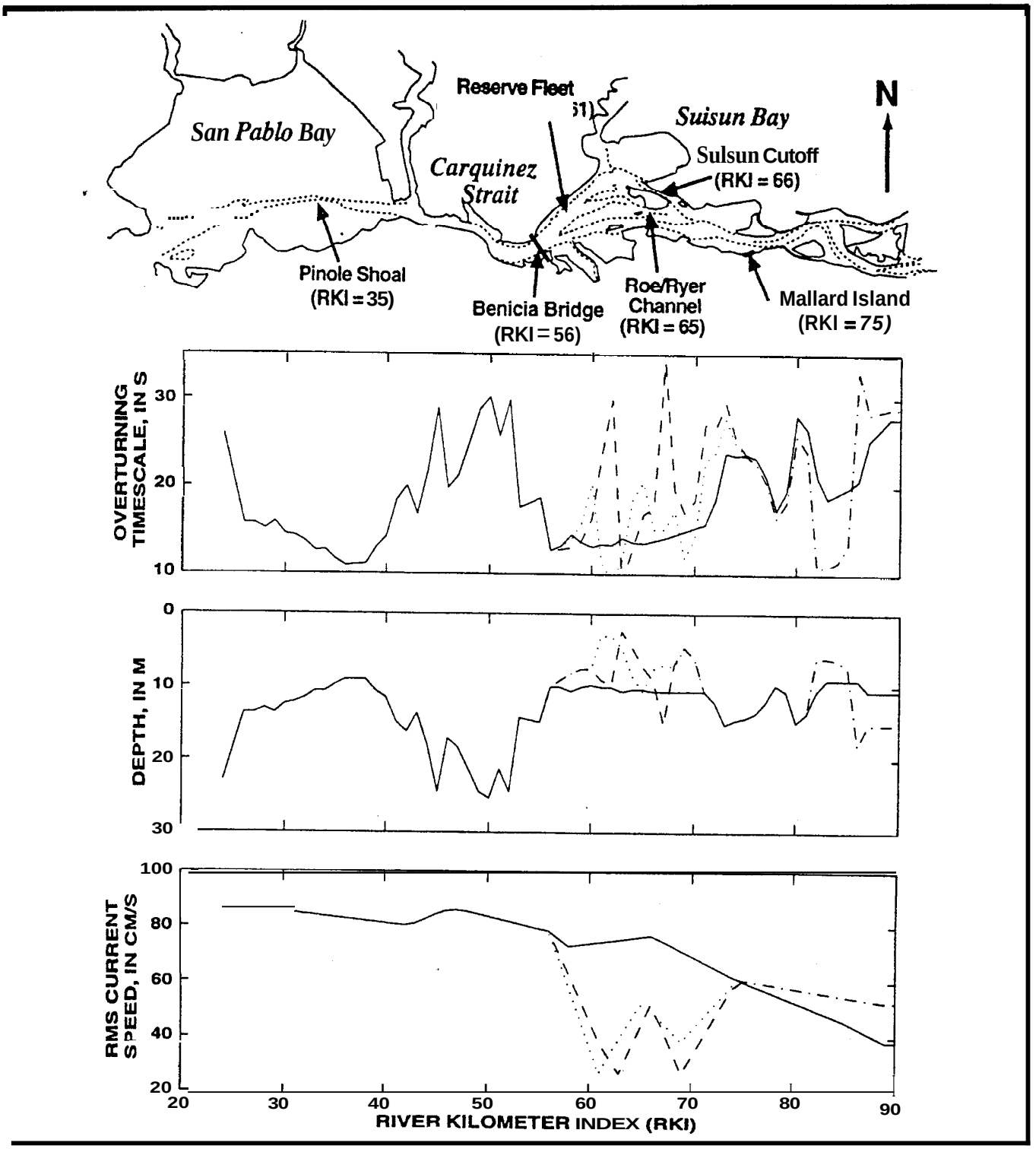

Figure 17

OVERTURNING TIMESCALE $\tau_0 = \frac{H}{U_s}$ ESTIMATED USING THE ROOT-MEAN-SQUARED NEAR-SURFACE CURRENT AND DEPTHS FROM ACOUSTIC DOPPLER CURRENT PROFILER DATA AS A FUNCTION OF ESTUARINE POSITION, SUISUN BAY

There are several distinct channels in Suisun Bay and the western delta; these channels are represented in this figure by different line types. The solid line represents the ship channel and the Sacramento River, the dashed line is the Reserve Fleet/Suisun Cutoff channel, and the dotted line is the Roe/Ryer Island Channel, and finally, the chain-dashed line represents the San Joaquin River. River kilometer index (RKI) is the channel distance in kilometers from the Golden Gate Bridge. (CM/S=centimeters per second; M=meters; S=seconds.)

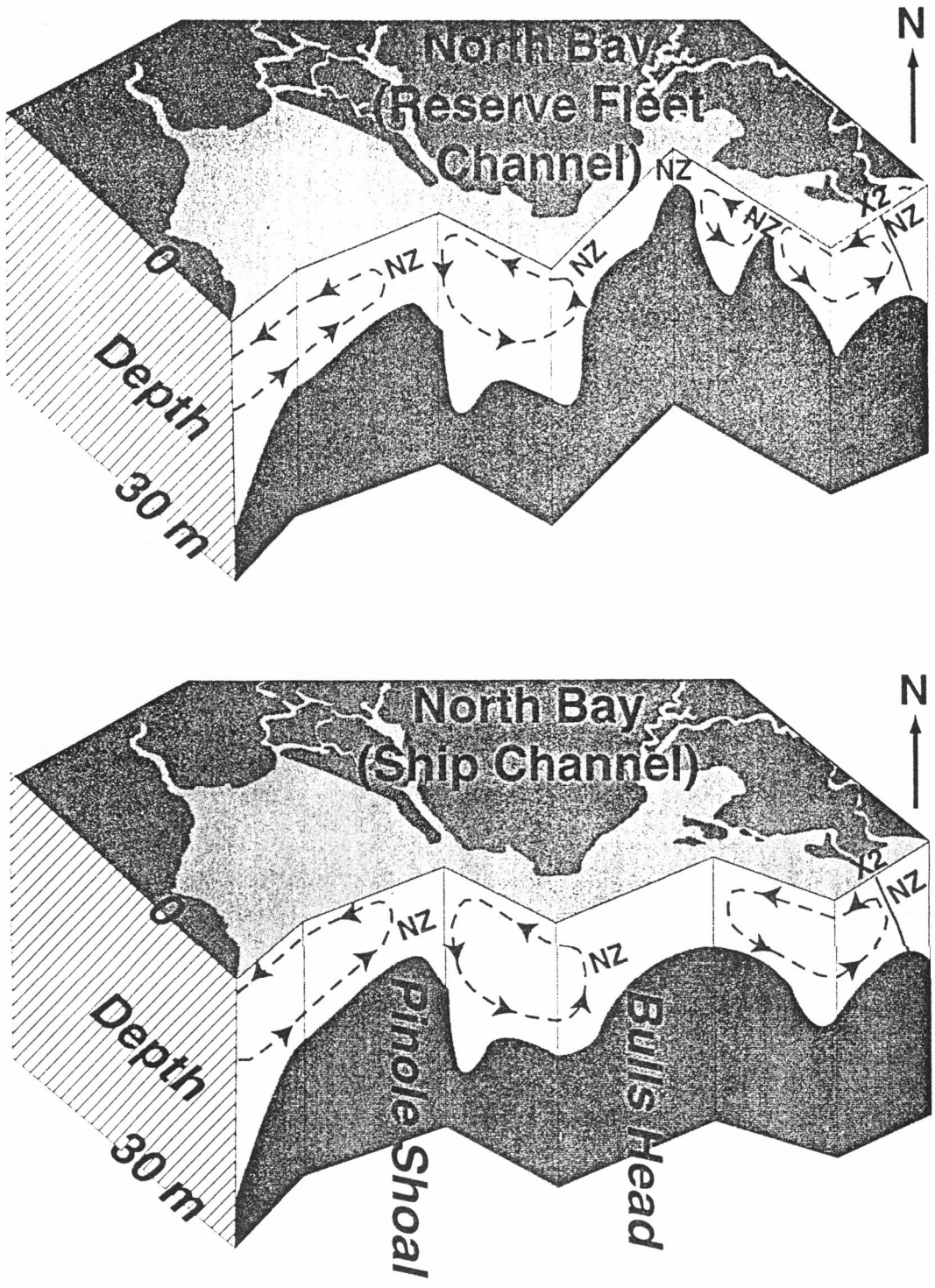

Figure 18

CONCEPTUAL MODEL OF GRAVITATIONAL CIRCULATION IN THE NORTH BAY, BASED ON THE OVERTURNING TIMESCALE

A longitudinal slice up the axis of the (a) Reserve Fleet/Suisun Cutoff channel and (b) the ship channel of Suisun Bay and the San Joaquin River are shown.

Salient features of this revised conceptual model of gravitational circulation include the possibility of multiple gravitational circulation cells that terminate near restrictions in depth and a modulation of gravitational circulation cell strength with the spring/neap cycle.

(NZ=null zone; M=meters.)

of bottom topography, gravitational circulation is always seaward of X2; therefore, X2 must be landward of each of the gravitational circulation cells shown in Figure 2-18 for the gravitational circulation cells to occur.

The overturning timescale not only varies in space, but can vary considerably with the fortnightly spring/neap cycle. According to Cheng and Gartner (1984), the maximum tidal current speed at spring tide can be estimated by (M2+S2) + (O1+K1), and the maximum speed at neap tide is estimated to be not less than (M2+S2) + (O1+K1) where M2, S2, O1, and K1 are the principal partial tides computed from harmonic analysis. By using these estimates for the spring and neap tidal currents, a large variation in the tidal currents exists between spring and neap tides, which, in turn, affects the overturning timescale shown in Figure 2-19. Because

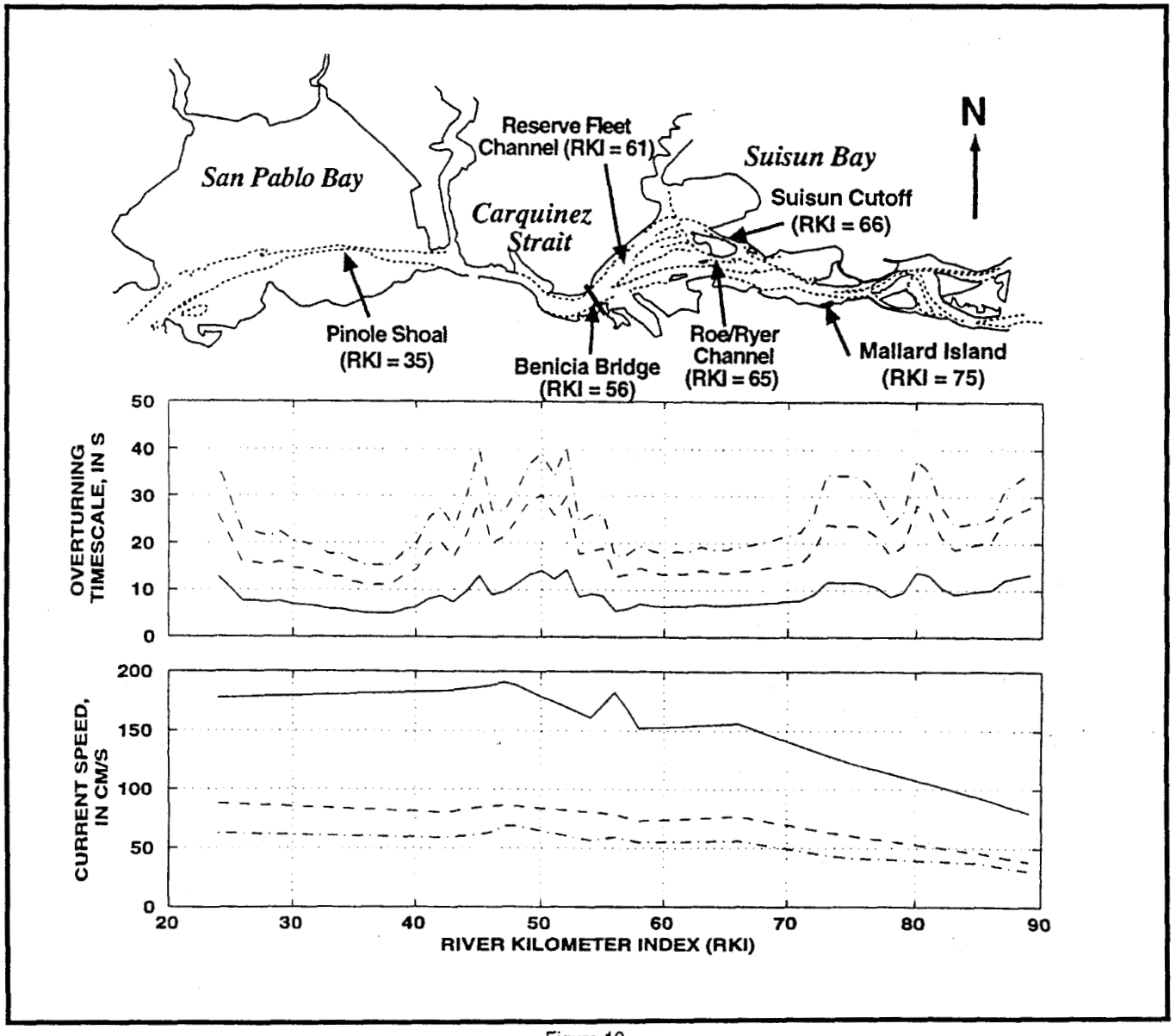

Figure 19
OVERTURNING TIMESCALE AND CURRENT SPEED DURING SPRING CURRENT MAXIMUMS (solid), ROOT-MEAN-SQUARED CURRENT (dash), AND NEAP CURRENT MINIMUMS (dash-dot), SACRAMENTO RIVER TO SUISUN BAY
River kilometer index (RKI) is the channel distance in kilometers from the Golden Gate Bridge.
(CM/S=centimeters per second; S=seconds.)

the overturning timescale is squared in the horizontal Richardson number, a factor of two difference in the overturning timescale means a factor of four difference in the Richardson number.

Stratification Timescale

The low-pass-filtered salinities at Mallard Island and the low-pass-filtered basin-wide horizontal salinity gradient, $\frac{\partial S}{\partial x}$ (see appendix for the computational details), are shown in Figure 2-20. The time mean horizontal salinity gradient is highly variable throughout the winter-spring period, depending on delta outflow for a given year. Even though 1992, 1993, and 1994 represent significantly different water year types, the basin-wide horizontal salinity

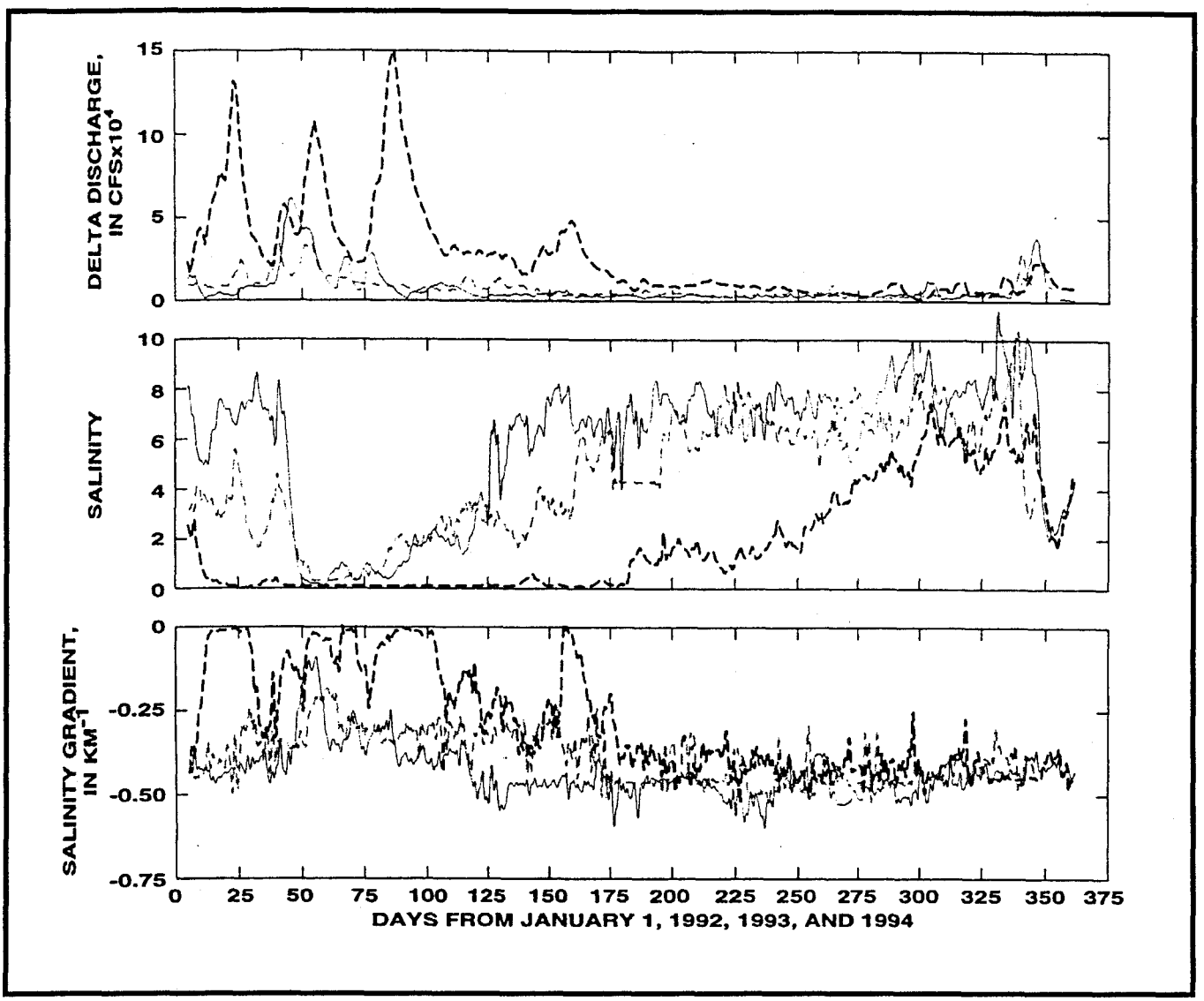

Figure 20
TIME SERIES PLOTS OF DELTA OUTFLOW (DAYFLOW) (top), MALLARD ISLAND LOW-PASS-FILTERED SALINITY (middle), AND THE BASINWIDE HORIZONTAL LOW-PASS-FILTERED, NEAR-BED SALINITY GRADIENT, dS/dx, (bottom) FOR 1992 (solid), 1993 (light dash), AND 1994 (dark dash), MALLARD ISLAND.

The horizontal salinity gradient is computed by taking the difference between the Mallard Island near-bed salinity and subtracting it from the Martinez near-bed salinity divided by the distance between the station locations. The units in the middle and lower panel could have been given as psu per kilometer, but salinity has no units (see glossary). (KM=kilometer; CFS= cubic feet per second.)

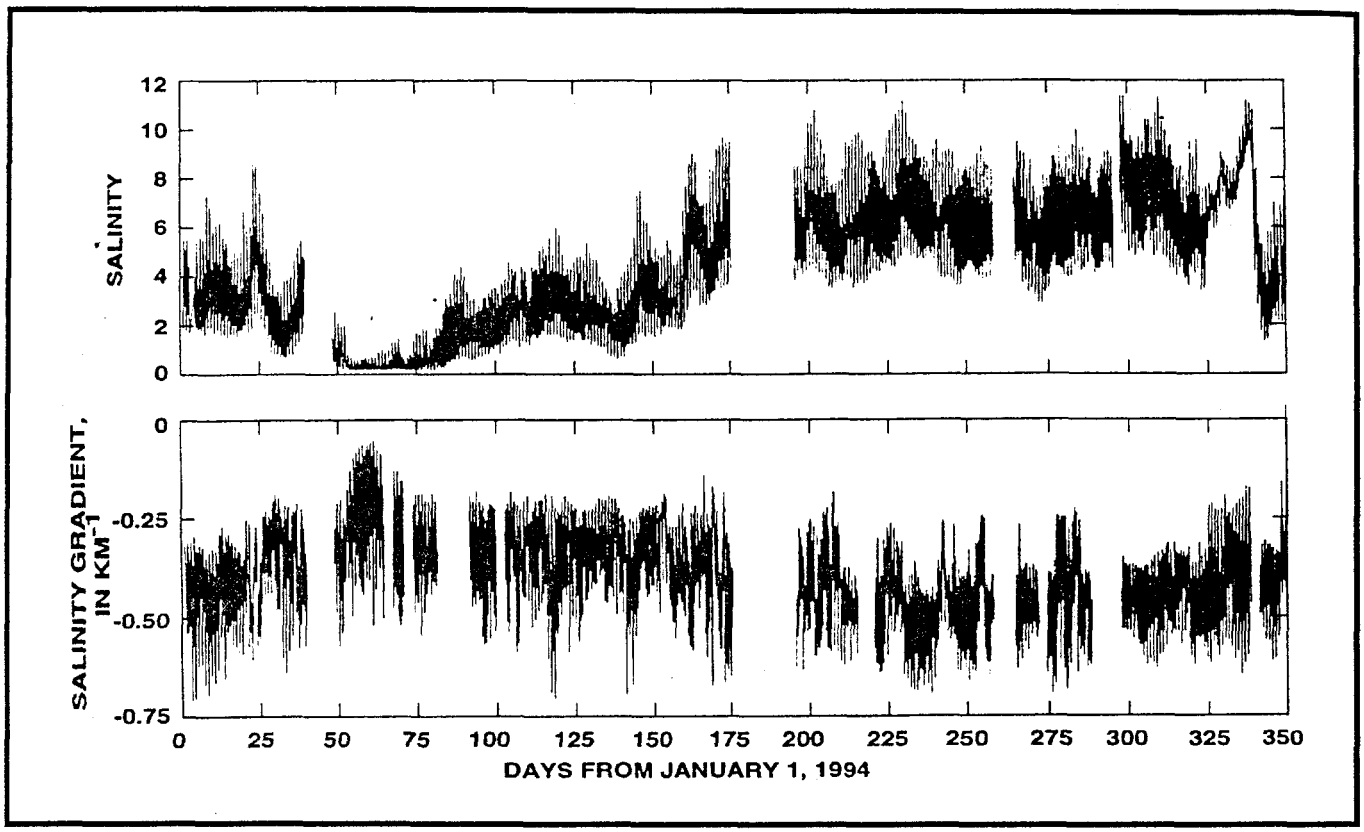

Figure 21
TIME SERIES PLOTS OF SALINITY (top) AND THE BASINWIDE HORIZONTAL SALINITY GRADIENT, dS/dx, (bottom), MALLARD ISLAND

The basinwide horizontal salinity gradient fluctuates tidally. The units in the lower panel could have been given as psu per kilometer, but salinity has no units (see glossary.) (KM=kilometer.)

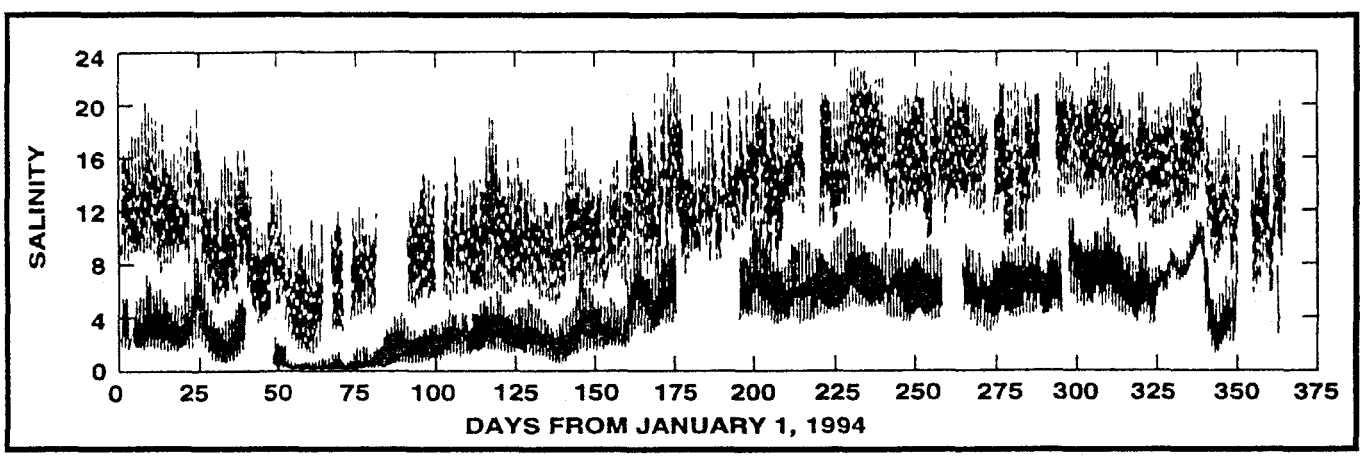

Figure 22
TIME SERIES PLOTS OF THE SALINITIES AT MARTINEZ (dash) AND MALLARD ISLAND (solid)

The tidal variation in salinity is much greater at Martinez. Salinity has no units (see glossary).

gradient, on which the stratification timescale depends, approaches about 0.4 psu/km in late summer-early autumn during each year. The large tidal fluctuations in the horizontal gradients shown in Figure 2-21 are due, in part, to the much larger tidal fluctuation in salinity at Martinez (Figure 2-22). The basinwide and the local horizontal salinity gradients are nearly always greater on flood than on ebb in Suisun Bay, indicating a contraction of the salt field on flood and an expansion on ebb because of the greater change in salinity over the tidal cycle at Martinez than at Mallard Island $\frac{\partial S}{\partial t}Mart > \frac{\partial S}{\partial t}Mal.$ This expansion and contraction is due to a combination of the greater velocities at Martinez over Mallard Island $U_{Mart} > U_{Mal}$ and the horizontal salinity gradient at Martinez is greater than the basin-wide mean horizontal salinity gradient, which, in turn, is greater than the gradients at Mallard Island

$$\frac{\partial S}{\partial \chi}Mart > \frac{\partial S}{\partial \chi}Basin > \frac{\partial S}{\partial \chi}Mal.$$

The time variability in the basinwide horizontal salinity gradient suggests that this gradient may be useful in looking at long-term trends, but is of little use in studying local dynamics because the local horizontal salinity gradient also is tidal timescale dependent and likely different than the basin mean shown in Figure 2-20.

As previously discussed, the horizontal salinity gradients at a given location can vary tidally, but fortnightly and seasonal variations also are important in understanding when and where gravitational circulation occurs. For example, several roughly four-fold increases in the horizontal salinity gradient during neap tides were observed during summer 1995 in Suisun Cutoff (Figure 2-23).

The low-pass-filtered surface current squared, $\overline{u^2}$, is a measure of the tidal energy. Peaks in $\overline{u^2}$ are spring tides, and valleys correspond to neap tides. In Figure 2-23, the neap tides correspond directly to increases in the horizontal salinity gradient (but with a noticeable time lag).

Seasonal variations in the time-mean horizontal salinity gradient also have been observed. Figure 2-24 plots low-pass-filtered salinity, which generally increases as the summer and autumn progress, as a function of the horizontal salinity gradient. Although there are many physical forcing mechanisms that control S and $\frac{\partial S}{\partial x}$, the $\frac{\partial S}{\partial x}$ magnitude increases as salt intrudes into the system.

In summary, gravitational circulation is dependent primarily on the horizontal salinity gradient that varies seasonally with the position of the salt field. The position of the salt field depends primarily on the uncontrolled winter inflows from the delta; however, the horizontal gradients in the salt field also appear to have a secondary dependence on local effects (primarily bathymetry) and the spring/neap cycle. The spatial distribution of gravitational circulation also depends strongly on the ratio of the tidal currents to the depth, or overturning timescale given in Figure 2-17. On the basis of this timescale, gravitational circulation is likely to occur in the Reserve Fleet Channel and Suisun Cutoff and landward of Mallard Island, and null zones are predicted to occur at Pinole Shoal (needs to be confirmed with data), the Benicia Bridge, and the shallow areas northeast and southwest of Suisun Cutoff (these also need to be confirmed with data) when the time mean position of X2 is significantly landward of these locations.

Our revised conceptual model of the north bay, based on Eulerian measurements, is as follows:

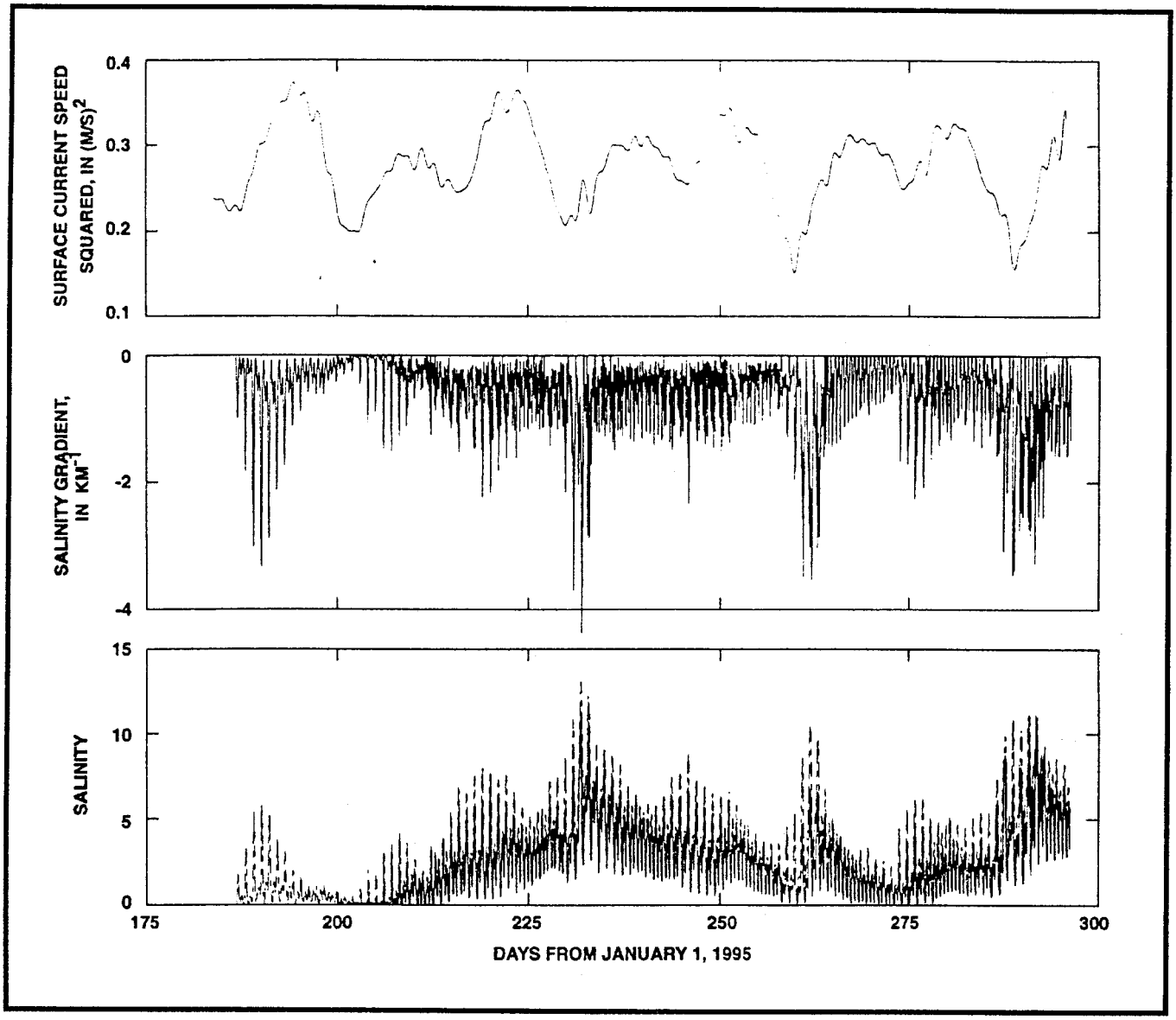

Figure 23
TIME SERIES PLOTS OF THE LOW-PASS-FILTERED ALONG-CHANNEL COMPONENT OF THE SURFACE CURRENT SQUARED, $\overline{u^2}$ (top), THE LOCAL HORIZONTAL SALINITY GRADIENT, dS/dx, IN SUISUN CUTOFF AS COMPUTED BY CONDUCTIVITY/TEMPERATURE INSTRUMENTS DEPLOYED 1.5 KILOMETERS APART ALONG THE AXIS OF SUISUN CUTOFF (middle), AND THE SALINITY IN SUISUN CUTOFF (bottom).
The bottom sensor is represented by the solid line and the surface sensor by the dashed.
The units in the middle panel could have been given as psu per kilometer, but salinity has no units (see glossary).
(KM=kilometer; M/S= meters per second; $(M/S)^2$ = square meters per second.)

- A semipermanent null zone (and possibly a turbidity maximum) is located near the Benicia Bridge during spring. At the very least, net near-bed currents are reduced significantly in the channels of western Suisun Bay from what they are in Carquinez Strait. Based on the horizontal Richardson number scaling, geographically fixed null zones also may exist in the shoal between the Reserve Fleet Channel and Suisun Cutoff and in the shoal south of Honker Bay (see the null zone designations on Figure 2-2 and the conceptual model in Figure 2-18).

- The inverse relation to velocity squared, U^2, in equation 1 accounts for the spring-neap modulations in gravitational circula-

tion strength (Burau and others 1993). The velocity squared is an index of the tidal energy available for vertical mixing. Increased vertical mixing from the increased tidal energy available during spring tides breaks down stratification, which effectively short circuits the gravitational circulation-induced two-layer flow.

- The horizontal density gradient, $\frac{\partial \rho}{\partial x}$, drives the gravitational circulation; without it, by definition, gravitational circulation does not exist.

Alternate Entrapment Mechanisms

Given gravitational circulation was not measured in Suisun Bay during the spring of 1992 and 1994, what does this imply about the existence of a turbidity maximum or entrapment zone based on existing conceptual models? Numerous publications (Arthur and Ball 1979; Peterson and others 1975, among others) have explained the turbidity maximum as resulting from a hyrodynamic null zone. The lack of measured net landward bottom currents in Suisun Bay during spring suggests that if a turbidity maximum or entrapment zone does exist during the spring, a mechanism other than gravitational circulation must be responsible. The low-salinity region of the estuary is also characterized by abundance maxima of several species of planktonic organisms (Kimmerer, this volume), and maxima in the proportion of bacteria that are attached to particles (Hollibaugh, this volume). Entrapment mechanisms must, therefore, explain not only maxima in concentration of particles (for example, turbidity) but also maxima in organism abundance. In the remaining sections, several possible entrapment mechanisms are discussed from a hydrodynamic perspective.

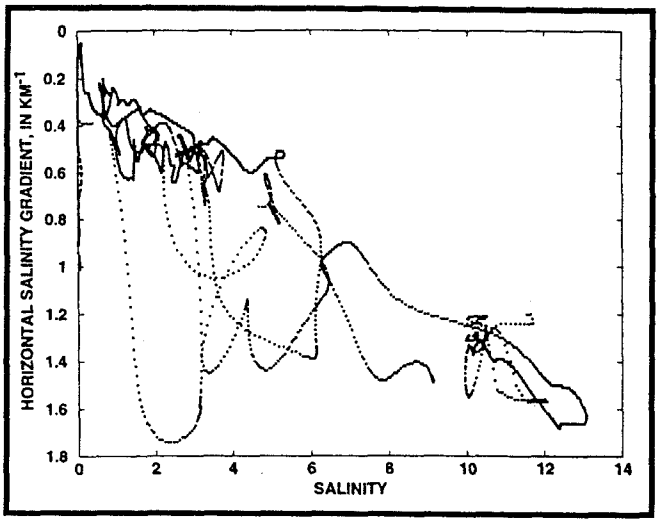

Figure 24
HORIZONTAL SALINITY GRADIENT DATA VERSUS TIDALLY-FILTERED SALINITY CONDUCTED AT SUISUN CUTOFF, DURING AUTUMN 1994 AND SPRING 1995.
The units in this figure could have been given as psu per kilometer, but salinity has no units (see glossary). (KM=kilometer.)

Vertical Migration

Because gravitational circulation is rare in Suisun Bay, three possible entrapment mechanisms are discussed that involve the correlation between the vertical distribution of organisms (or suspended solids) and vertical shear. The first two mechanisms discussed that could account for increased concentrations near X2 do not involve the assumption of biological behavior, but instead rely completely on the physics of shear-buoyancy interaction. These mechanisms are differentiated from each other, for the purposes of discussion, by the exact timing between the vertical concentration distribution (whether it be organisms or suspended solids) and the vertical shear, even though both mechanisms evolve from the same highly nonlinear interaction between the salt field and vertical mixing.

The first mechanism discussed simply requires the centroid of the concentration distribution to be higher in the water column during flood tides than during ebb tides. There are two possible ways (that we know of) in which the centroid of the concentration distribution can shift vertically

over the tidal cycle: one includes biological behavior, which is discussed in Kimmerer and Bennett (this volume): the other, a purely physical mechanism, is discussed in this chapter. In terms of suspended sediment transport, preliminary evidence suggests that there may be greater resuspension of bottom sediment in the channels during flood. tides than during ebbs in a stratified water column because the near-bed shear stress appears to be greater during flood (Stacey 1996). Moreover, increased near-bed shear during flood would also suggest that organisms attached to the bed or that are trying to remain near the bed would have a more difficult time remaining on or near the bed during flood in the presence of a horizontal salinity gradient. Therefore, ebb/flood asymmetry in the near-bed shear is a purely physical explanation that could explain increased flood water column concentrations over ebb, and could thereby explain a vertically averaged net landward transport of suspended sediment and biota at locations seaward of X2.

A conceptually satisfying outcome of this mechanism is that the ebb/flood asymmetry in the near-bed shear would end just seaward of X2, where the horizontal salinity gradient, for practical purposes, ends, which means the positive correlation between elevated water column concentrations and the flood tidal current would also end near X2. This purely physical mechanism could, therefore, explain the observed accumulations of suspended sediment and biota near the low salinity zone. Collaborative studies between the USGS (David Schoellhamer and Jon Burau) and Stanford University (Stephen Monismith, Matthew Brennan, and Jessica Lacy) of this mechanism, with respect to suspended in sediment transport, are currently (1998) under way.

The second purely physical mechanism that could account for accumulations near X2 depends on a sequence of tidally driven shear-buoyancy interactions in the presence of a weak horizontal salinity gradient. Although this mechanism is related to the first, it is different because all of the action occurs during a short (1- to 4-hour) interval around low slack water and the subsequent flood tide. The sequence is as follows:

(1)the water column naturally tends to become stratified during ebb tides through a process known as Strain Induced Periodic Stratification or SIPS (Simpson and others 1990). Weaker vertical mixing that occurs near slack water permits (a)a two-layer density driven exchange flow to occur that further stratifies the water column and (b) negatively buoyant particles to accumulate in the lower part of the water column through settling.

(2) During the period of weak vertical mixing near low slack water, a 1-to 4-hour density driven exchange flow advects the elevated concentrations of particles near the bottom landward. This intermittent advective process could ultimately lead to a net landward transport of particles up to a position near X2, where stratification dynamics cease to play an important role. The two-layer density driven flow is limited to slack water because the intense vertical mixing that occurs during the tidal current maximums breaks down stratification, which effectively short-circuits the density driven exchange flow.

The third and final vertical transport mechanism discussed involves biological behavior. This process, which is limited to organisms that can swim, depends on the correlation between vertical shear and organism position. Kimmerer (this volume) and Bennett (thisvolume) present evidence for vertical movement of organisms on a tidal cycle, with abundance higher in the water column on the flood than on ebb. This pattern appears to be universal in those species residing in this part of the estuary, implying that it is important to position maintenance.

For an organism to achieve a net upstream movement from vertical migration in synchrony with the tides, the water column must be sheared. If the shear is weak, as it is in a vertically well-mixed water column, little net upstream movement is derived from vertical migration. Conversely, when the water column is stratified, large local shears develop near the density interface that could easily be exploited by organisms to position themselves within the estuary. The greater the vertical shear, the shorter the vertical migration is needed to achieve net upstream movement. If the flow is strongly stratified, organisms only have to travel through the salinity (density)interface: a distance that often can be measured in centimeters rather than meters. Moreover, if the vertical distance required to achieve net upstream movement is minimal, it suggests that either less effort is required for an individual organism or that weaker organisms can succeed in achieving a net upstream benefit from vertical migration. In this section, the magnitude and timing of the stratification and shear in the ship channel in Suisun Bay is described in support of the vertical migration hypothesis.

Because flow reversals occur twice daily, differentiating between shear created on flood or ebb is desirable. For this chapter, the tidal current direction is based on the depth average currents where the shear is computed using the following relation:

$$\Delta U = \frac{\overline{U}}{|\overline{U}|}\left|U_S - U_B\right| \qquad (6)$$

where $|U_S - U_B|$ gives the magnitude of the shear and is strictly positive by definition and the term $\frac{\overline{U}}{|\overline{U}|}$ is either +1 or -1 when the depth-averaged, along-channel currents are flooding or ebbing, respectively. U_S, U_B, and $\overline{U}$ are the near-bed, near-surface, and depth-averaged currents, respectively.

The near-bed and near-surface salinities, the along-channel speeds, and ΔU are plotted in Figure 2-25, which shows a typical tidal cycle when locally weak salinity gradients were present. The timing of the shear and stratification is markedly different when the horizontal density gradient is strong (for example, strong enough to produce a gravitational circulation cell).

The water column rapidly stratifies as the flood begins to decelerate and continues to stratify through high water slack. The water column begins to destratify as the ebb begins to accelerate. Stratification reduces the vertical transfer of along-channel momentum causing a partial decoupling of the upper layer from the lower layer: thereby, increasing the shear in the water column. Even though stratification starts with the flood [in contrast to a strain-induced periodic stratification (SIPS) model], the greatest stratification and concomitant shear ΔU, occurs during the acceleration phase of the ebb (negative along-channel speed).

This pattern of stratification, with most of the shear occurring on ebb, is shown on Figure 2-26, where the bottom panel shows that the low-pass-filtered (tidally averaged) vertical shear is negative (for example, the shear occurs on ebb because of the way the shear in equation 6 is computed). If suspended-sediment concentrations, or biota, were to concentrate in the lower layer during stratification, their progress down-estuary would be considerably less (by about 50 cm/s for –3 hours or –5.5 km near day 146.25 in Figure 2-25) than the upper layer during this period. If suspended sediment, or biota, were concentrated in the lower layer during these times, and, if the concentrations could then become evenly distributed throughout the water column or were con-

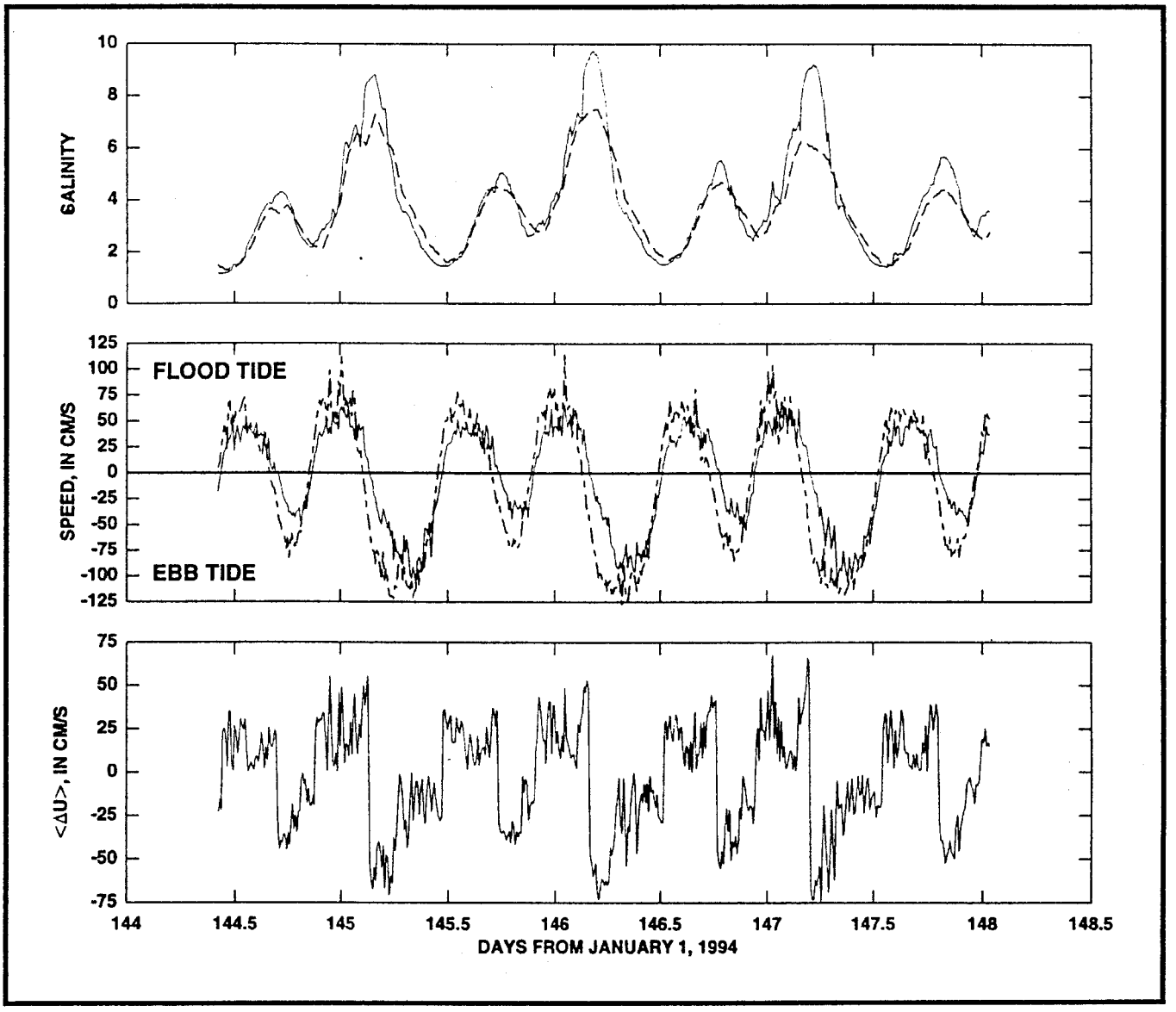

Figure 25
TIME SERIES PLOTS OF THE NEAR-BED (solid) AND NEAR-SURFACE (dash) SALINITIES (top);
THE NEAR-BED (solid) AND NEAR-SURFACE (dash) ALONG-CHANNEL SPEED (middle);
AND THE FLOOD/EBB NORMALIZED SHEAR (bottom) AT MALLARD ISLAND
The units in the middle and bottom panels could have been given as psu per kilometer, but salinity has no units (see glossary). (CM/S=centimeters per second).

centrated in the upper layer during the remainder of the tidal cycle, a vertically averaged, landward net flux could be achieved (depending on the thickness and concentration in the lower layer).

The conditions for this upstream migration mechanism would abruptly end near X2, where dynamically significant salinities and the increased shear that occurs on ebb cease to exist. Because the water column naturally mixes vertically during the tidal current maximums, the only unknowns in this alternate entrapment process are (1) whether elevated concentrations actually occur in the lower layer when the water column is stratified, and (2) the thickness of the lower layer. Zooplankton (Kimmerer, this volume) and larval fish (Bennett, this volume) appear to migrate vertically such that abundance is higher in the upper layer on the flood and higher in the lower layer on ebb. For copepods, this migration appears to be insufficient, at

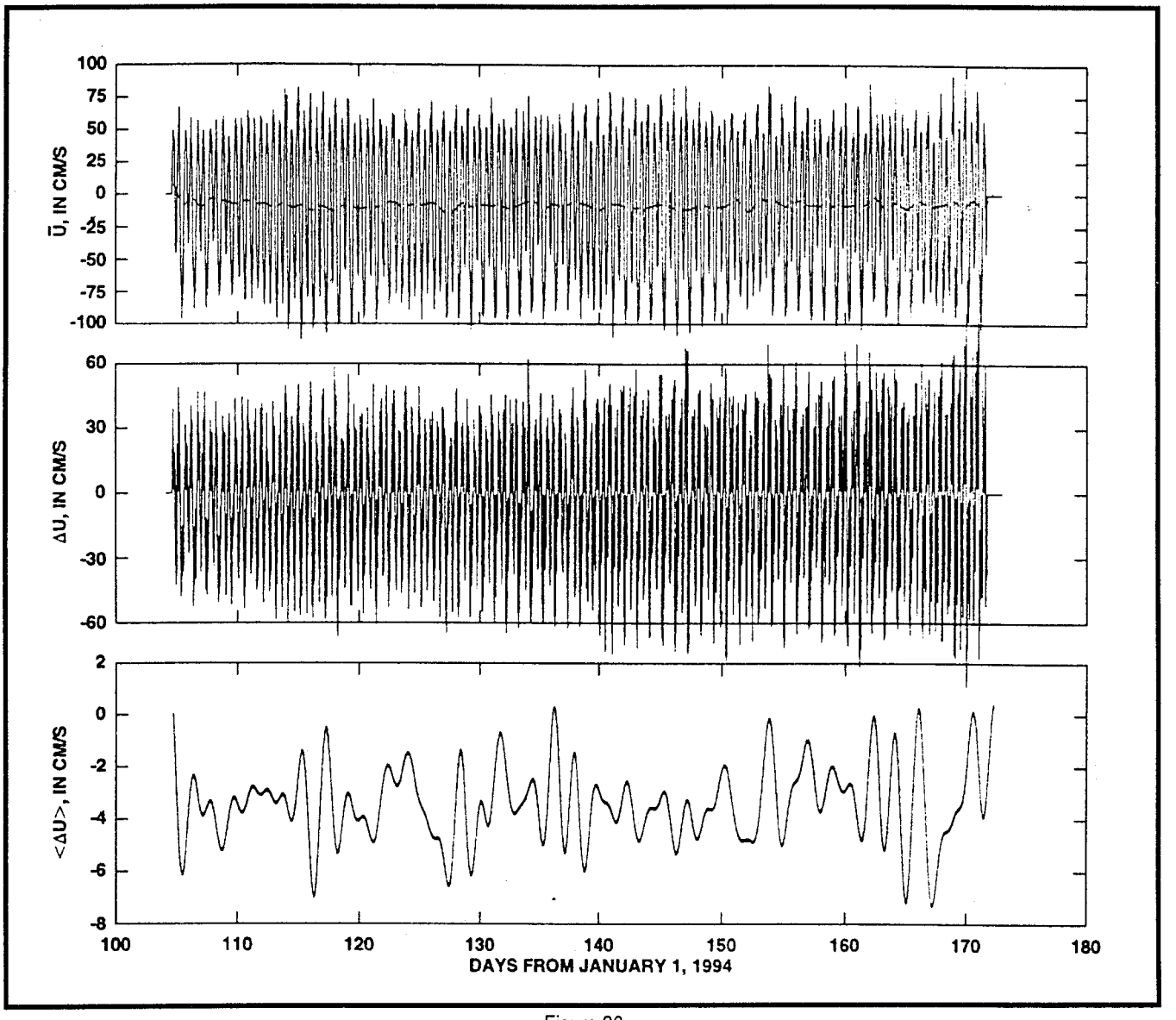

Figure 26
TIME SERIES PLOTS OF THE DEPTH-AVERAGED, ALONG-CHANNEL CURRENT ($\overline{U}$); THE VERTICAL SHEAR (ΔU); AND THE TIDALLY AVERAGED VERTICAL SHEAR, ($<\Delta U>$), AT MALLARD ISLAND
(CM/S=centimeters per second.)

least for the period of our data collection, to overcome the net transport (Kimmerer, this volume), because of the weak stratification and concomitant shear referred to above. An alternate migratory mechanism appears to exist for mysids and amphipods (Kimmerer, this volume) by which these organisms are apparently less abundant throughout the water column on ebb than on flood. If they are on the bottom on ebb, where seaward transport would be negligible, their migratory behavior could overcome the lack of vertical shear and result in net landward movement (Kimmerer, this volume).

Stokes' Drift

An upstream residual current, Stokes' drift, can occur in progressive wave systems like the north bay of San Francisco Bay. Stokes' drift creates a flux in the direction of wave propagation that evolves from the correlation of sea level and the

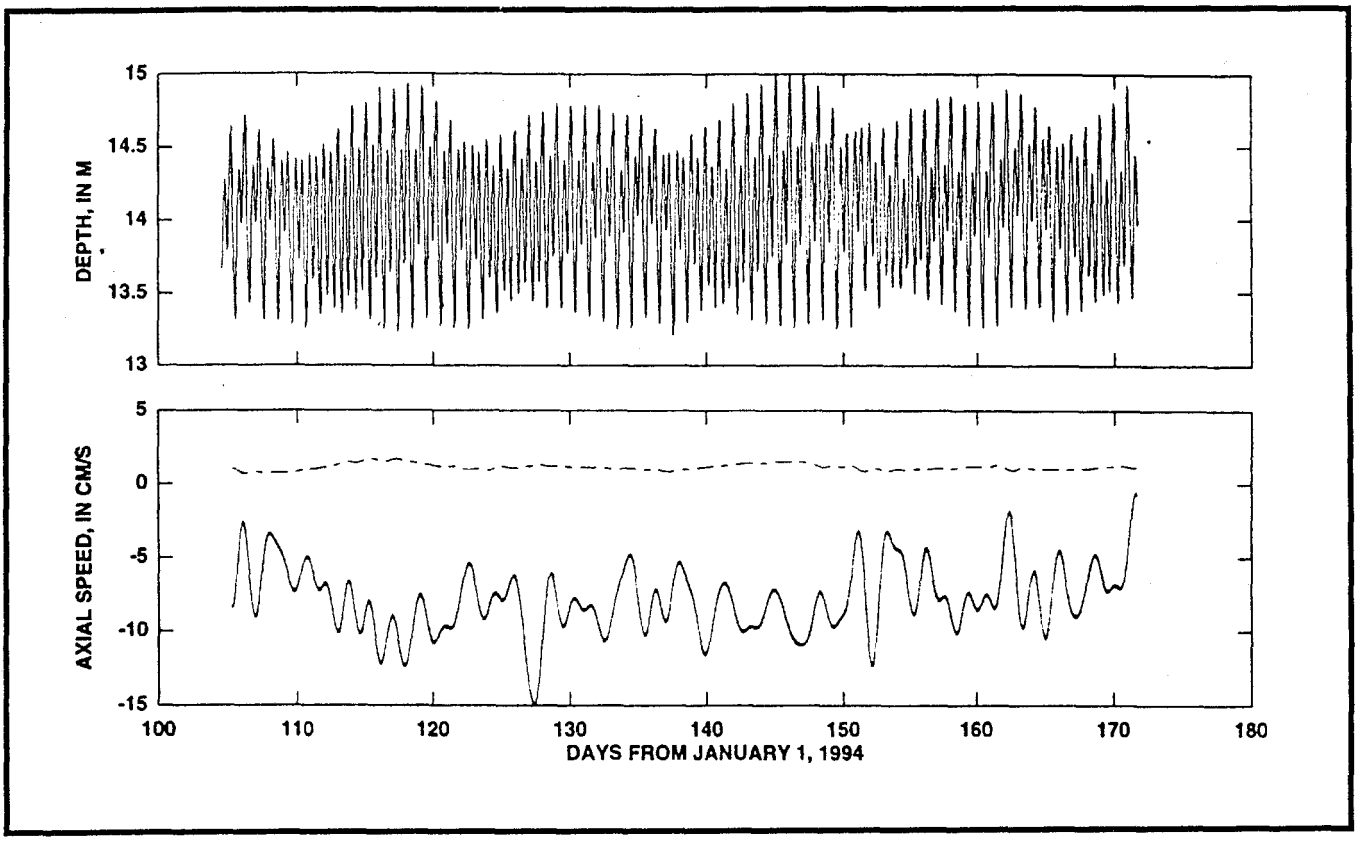

Figure 27
TIME SERIES OF DEPTH AT MALLARD ISLAND, (top) AND THE LOW-PASS-FILTERED, DEPTH-AVERAGED, ALONG-CHANNEL SPEED (bottom, solid) AND THE STOKES' DRIFT VELOCITY (bottom, dashed)
(CM/S=centimeters per second; M=meters.)

tidal current. For example, the residual (time average) mass flux past an ADCP location is

$$<\bar{u}H>=<\bar{u}>h+<\bar{u}'\zeta> \qquad (7)$$

where $\bar{u}=<\bar{u}>+\bar{u}'$ is the depth-averaged velocity, H = h + ζ is the total depth, h is the tidally averaged depth, and ζ is sea level where the operators (<>, ′) represent a time average and the tidal fluctuation components, respectively. The overbar represents a depth average.

Dividing the Stokes' drift by the time-mean depth allows the Stokes' drift to be cast in terms of a velocity. The time-mean, depth-averaged velocity, $<\bar{u}>$, and the Stokes' drift velocity, $\frac{<\bar{u}'\zeta>}{h}$, are shown in Figure 2-27. The Stokes' drift profile is vertically nonuniform (Ianniello 1977), and simple modeling studies indicate that the vertical Eulerian velocity profile attributed to Stokes' drift is strictly positive (landward) throughout the water column (Najarian and others 1984) (Figure 2-3). To compute the Stokes' drift profile from data, estimates of the stream-wise velocity, the vertical and along-channel derivatives in the stream-wise velocity, and the vertical velocity component are needed. These parameters could not be measured in 1994 with the instrumentation available at that time; therefore, the Stokes' drift contribution could not be vertically partitioned. Nonetheless, the depth-averaged Stokes' drift velocity is small (<2 cm/s) with greater magnitudes on spring tides than on neap tides (Figure 2-27), which is consistent with previous research (Walters and Gartner 1985).

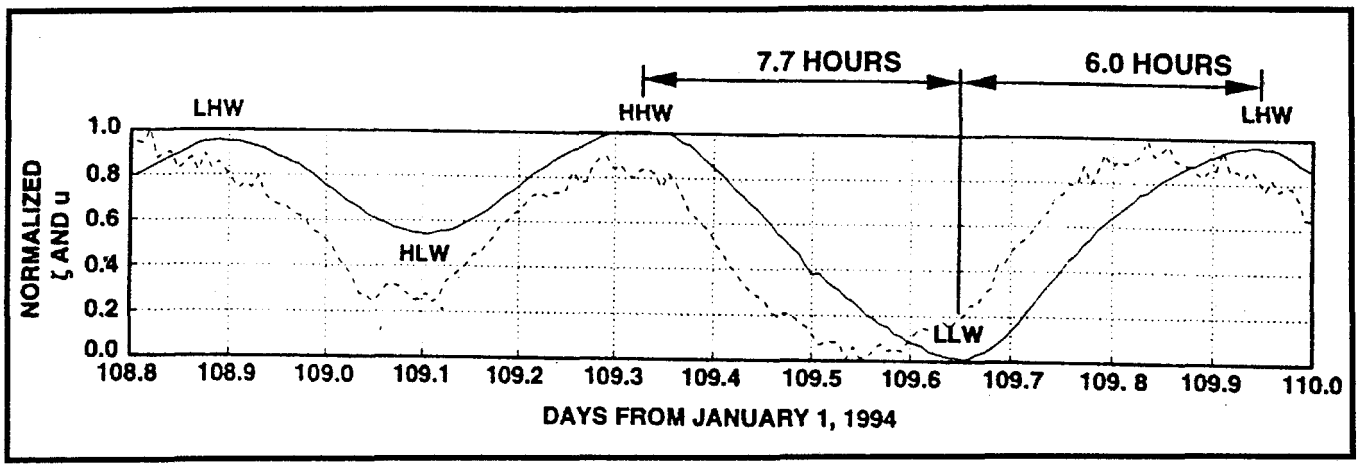

Figure 28
NORMALIZED SEA LEVEL, ζ (solid), AND DEPTH-AVERAGED VELOCITY, *u* (dashed), AT MALLARD ISLAND
The abbreviations, from left to right, are: LHW, lower high water; HLW, higher low water; HHW, higher high water; LLW, lower high water.

Two things are relevant in determining whether Stokes' drift is important: (1) the magnitude of the tidal range, ζ , relative to the mean depth, h (if $\frac{\zeta}{h} << 1$, Stokes' drift is not important), and (2) the phase between the tide (sea level) and the tidal current. If the phase between the tide and tidal currents is 90 degrees (standing wave), then the sea-level variations and the currents are uncorrelated and Stokes' drift is not important. Conversely, if the phase between the tide and tidal current is 0 degrees, then the tide and tidal currents are perfectly correlated and Stokes' drift may be important depending on the magnitude of $\frac{\zeta}{h}$. Using Mallard Island data as an example, the tidal range is ζ = 1.2 m and the mean depth is h = 13 m, so $\frac{\zeta}{h} << 1$.

The idea of a purely progressive or purely standing wave system is a conceptual construct. In real estuarine systems, the phase between the tides and the tidal currents changes spatially and temporally. The normalized sea level and along-channel velocities at Mallard Island for a typical tidal cycle are shown in Figure 2-28. These time series are normalized so they can be overlaid and easily compared. The timing of the tidal currents, relative to the tide, changes over the tidal cycle (Figure 2-28). For example, the decline from higher high water (HHW) to lower low water (LLW) takes 7.7 hours, whereas the rise from LLW to lower high water (LHW) takes 6.0 hours. Moreover, the shape of the decline is not only longer but more gradual than the rising tide, which shows evidence of wave steepening indicative of more rapid progress of LHW upstream. This tidal distortion is caused primarily by interaction between the incoming tidal currents and the outgoing time-mean current (delta outflow) (Godin 1991).

In terms of the phase between the tide and the tidal currents, the weak tides (day 108.8 to 109.35 in Figure 2-28) represent periods when sea levels are closer to being in phase (correlated) than they are during the strong tides (day 109.35 to 109.95 in Figure 2-28). The difference between the correlation during spring versus neap tides is shown in Figure 2-29 where the time difference between the tidal currents and sea level are plotted and in Figure 2-30 where the phase lag ($phase_{currents}$ - $phase_{tide}$), assuming a semidiurnal period of 12.42 hours (principal lunar component of the tide referred to as the M2 tide), is

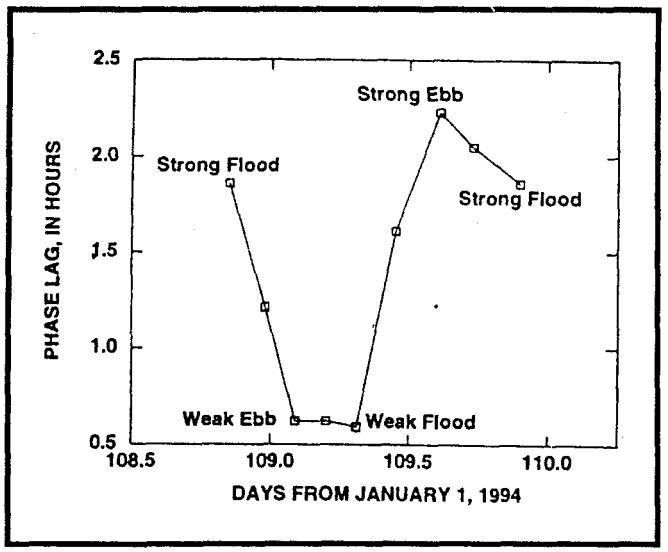

Figure 29
PHASE LAG ASSUMING A SEMIDIURNAL TIDAL PERIOD OF 12.42 HOURS (M2 tide) BETWEEN SEA LEVEL AND THE CURRENTS AT MALLARD ISLAND

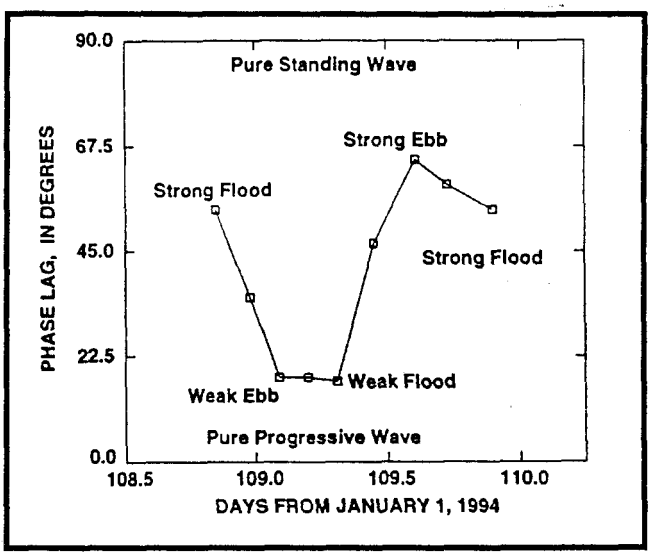

Figure 30
PHASE LAG, ASSUMING A SEMIDIURNAL TIDAL PERIOD OF 12.42 HOURS (M2 tide) BETWEEN SEA LEVEL AND THE CURRENTS AT MALLARD ISLAND

plotted. The tides and tidal currents in the north bay are, on average, only weakly correlated [ϕ_{ave} = 40°, $cos(40°)$ = 0.77]; the weakest correlation occurs during the period of maximum tidal exchange.

In summary, Stokes' drift is weak in Suisun Bay (Mallard Island specifically) because sea level variations are small relative to the mean depth ($\zeta << h$) and the correlation between sea level and the tidal currents is weak (particularly during the maximum flood and ebb periods).

Management Implications

The revised conceptual model of gravitational circulation presented in this paper has significant implications to proposed dredging in Suisun Bay and to the generally accepted hydrodynamic explanation for the turbidity maximum and the entrapment zone. Observation of residual currents and theoretical analysis of the horizontal Richardson number highlight the importance of bathymetry in the establishment of gravitational circulation cells. For example, proposed dredging of the John R. Baldwin and Stockton ship channels (U.S. Army Corps of Engineers 1989) would change the bathymetry near the Benicia Bridge (dredged from 11 m deep and 92 m wide to 14 m deep and 183 m wide). The horizontal Richardson number scaling discussed in this chapter suggests that deepening the ship channel in this area could locally increase gravitational circulation, which could result in elevated salinities in Suisun Bay and the western delta. However only a detailed hydrodynamic study of this area can quantify the effects of such dredging.

Acknowledgments

This study was done in cooperation with the San Francisco Bay ecosystem initiative of the USGS, DWR, and the USBR, as part of the Interagency Ecological Program. The authors greatly appreciate the help of Randall Brown (DWR) and Jim Arthur (USBR) in arranging the funding for this work. The guidance and encouragement from Steve Monismith, Jeffrey Koseff (Stanford University) and Ralph Cheng and Peter Smith (USGS) were essential in the design and execution of this study. The field study described in this chapter required the help of a number of people. Jim Burau; Rick Oltmann, Rick Adorador, and Scott Posey (USGS); and Doug Ball and Jim Arthur (USBR) put in many hours in the field to obtain the data.

Armi, L. 1986 The hydraulics of two flowing layers with different densities: *Journal of Fluid Mechanics*, v. 163, p. 27-58.

Arthur, J.F. and M.D. Ball. 1979. Factors influencing the entrapment of suspended material in the San Francisco Bay Estuary, Conomos, T.J., editor, *San Francisco Bay: The Urbanized Estuary*. San Francisco, Pacific Division, American Association for the Advancement of Science, p. 143-174.

Bowden, K.F. 1960. Circulation and mixing in the Mersey estuary. International Association of Scientific Hydrology Committee of Surface Waters, *Publication 51*, p. 352-360.

Buchanan, P.A., D.H. Schoellhamer, and R.C. Sheipline. 1996. Of suspended-solids concentration data, San Francisco Bay, California, water year 1994. U.S. Geological Survey *Open-File Report 95-776*, 48 p.

Burau, J.R., M.R. Simpson, and R.T. Cheng. 1993. Tidal and residual currents measured by an acoustic Doppler current profiler at the west end of Carquinez Strait, San Francisco Bay, California, March to November 1988. U.S. Geological Survey Water-Resources *Investigations Report 82-4064*, 79 p.

Cheng, R.T., V. Casulli, and J.W. Gartner. 1993. Tidal, residual, intertidal mudflat (TRIM) model and its applications to San Francisco Bay, California. *Estuarine, Coastal and Shelf Science*, v. 36, p. 235-280.

Cheng, R.T. and J.W. Gartner. 1984. Tides, tidal and residual currents in San Francisco Bay, California-Results of measurements, 1979-1980: pt. 2, Results of measurements in Suisun Bay region. U.S. Geological Survey Water-Resources *Investigations Report 84-4339*, 231 p.

Conomos, T.J., D.H. Peterson, D. S. McCulloch, and P.R. Carlson. 1971. Drift of surface and near-surface bottom waters of the San Francisco Bay system: March 1970 through April 1971. U.S. Geological Survey Open-File map.

Conomos, T.J. 1979. Properties of circulation of San Francisco Bay waters material in the San Francisco Bay Estuary, T.J. Conomos, editor. *San Francisco Bay: The Urbanized Estuary*. San Francisco, Pacific Division, American Association for the Advancement of Science, p. 47-84.

Denton, R.A. and J.R. Hunt. 1986. Currents in San Francisco Bay-Final report. University of California and Berkeley, *Hydraulic and Coastal Engineering Report No. UCB/HEL-86/01*, 99 p.

Downing, J.P. 1983. *An* optical instrument for monitoring suspended particulates in ocean and laboratory: Abstract, *OCEANS* 1983, San Francisco, California, August 29-September 1, 1983, p. 199-202.

Dyer, K.R. 1973. *Estuaries: A physical introduction.* New York, John Wiley, 140 p.

Farmer, D.M. and L. Armi. 1986. Maximal two-layer exchange over a sill and through the combination of a sill and contraction with barotropic flow: *Journal of Fluid Mechanics,* v. 164, p. 53-76.

Fischer, H.B., E.J. List, R.C.Y. Koh, J. Imberger, and N.H. Brooks. 1979. *Mixing in Inland and Coastal Waters.* Academic Press, New York, 483 pp.

Geyer, W.G. 1993. The importance of suppression of turbulence by stratification on the Estuarine Turbidity Maximum. *Estuaries,* v. 16, no. 1, p. 113-125.

Godin, G. 1991. Frictional effects in river tides, in Parker, Bruce, editor, *Tidal hydrodynamics.* New York, John Wiley, p. 379-402.

Hansen, D.V. and M. Rattray. 1965. Gravitational circulation in straits and estuaries. *Journal of Marine Research,* v. 23, p. 104-122.

Hill, K.D., T. M. Dauphinee, and D.J. Woods. 1986. The extension of the practical salinity scale 1978 to low salinities. Institute of Electrical and Electronics Engineers, *Journal of Oceanic Engineering,* v. OE-11, no. 1, p. 109-112.

Ingles, C. and F.H. Allen. 1957. The regimen of the Thames estuary. *Proceedings of the Institute of Civil Engineers (London),* v. 7, p. 827-868.

Jassby, A.D., W.M. Kimmerer, S.G. Monismith, C. Armor, J.E. Cloern, T.M. Powell, J. Shubel, and T. Vendlinski. 1995. Isohaline position as a habitat indicator for estuarine resources: San Francisco Bay-Delta, California, *U.S.A. Ecological Applications,* v. 5, p. 273-289.

Jay, J.A., B.S. Giese, and C.R. Sherwood. 1990. Energetics and sedimentary processes in the Columbia River estuary. *Prog. Oceanography,* v. 25, p. 157-174.

Kimmerer, W.M. 1993. An evaluation of existing data in the entrapment zone of the San Francisco Bay Estuary. Biosystems Analysis, Inc., *Technical Report 33,* 49 p.

Millero, F.J. 1993. What is a psu? *Oceanography,* v. 6, no. 3, p. 67.

Monismith, S.G., J.R. Burau, and M. Stacey. 1996. Hydrodynamic transport and mixing processes in Suisun Bay, Hollibaugh, J.T., editor, *San Francisco Bay: The Ecosystem* San Francisco, Pacific Division, American Association for the Advancement of Science, p. 123-153.

Mortenson, W.E. 1987. Investigation of estuarine circulation in Suisun Bay: The Bay Institute of San Francisco Exhibit 49, *State Water Resources Control Board Hearing 13,* 70 p.

Najarian, T.O., D.P. Wang, and P.S. Huang. 1984. Lagrangian transport model for estuaries. American Society of Civil Engineers, *Journal of Waterway, Port, Coastal and Ocean Engineering,* v. 110, no. 3, p. 321-333.

Nichol, G.D. 1996. Estuarine circulation cell of lower Sacramento River: Reno, University of Nevada, Ph.D. thesis, 197 p.

Nichols, M., and G. Poor. 1967. Sediment transport in a coastal plain estuary. American Society of Civil Engineers, *Journal of Waterways and Harbors Division,* v. 93, p. 83-95.

Nunes Vaz, R.A., G.W. Lennon, and J.R. de Silva Samarasinghe. 1989. The negative role of turbulence in estuarine mass transport. *Estuarine, Coastal and Shelf Science,* v. 28, p. 361-377.

Officer, C.B. 1976. *Physical oceanography of estuaries (and associated coastal waters).* New York, John Wiley, 465 p.

Peterson, D.H., T.J. Conomos, W.W. Broenkow, and P.C. Doherty. 1975. Location of the nontidal current null zone in northern San Francisco Bay. *Estuarine and Coastal Marine Science,* v. 3, p. 111.

Postma, H., and K. Kalle. 1955. One the development of turbid zones in the lower course of rivers with a special consideration of the conditions in the lower Elbe. Sonde. *Deutche Hydr. Zeitschrift,* v. *8,* p. 137-144.

Pritchard, D.W. 1952. Salinity, distribution, and circulation in Chesapeake Bay estuarine system. *Journal of Marine Research,* v. 11, p. 106-123.

Schubel, J.R. 1968. Turbidity maximum of northern Chesapeake Bay. *Science,* 8, v. 161, p. 1013-1015.

Simpson, J.H., J. Brown, J. Mathews, and G. Allen. 1990. Tidal straining, density currents, and stimng in the control of estuarine stratification. *Estuaries,* v. 13, no. 2, **p.** 125-132.

Smith, L.H. 1987. **A** review of circulation and mixing studies of San Francisco Bay California. U.S. Geological Survey *Circular* 1015, 18 p.

Smith, T.A., and G.V. Bogle. 1993. Three dimensional particle tracking model for the Sacramento-San Joaquin Delta. *Proceedings, American Association of Civil Engineers Hydraulic Engineering Conference,* San Francisco, California, p. 827-832.

Stacey, M.T. 1996. Turbulent mixing and residual circulation in a partially stratified estuary: Stanford University, California, Ph.D. thesis, 209 p.

UNESCO. 1985. The international system of units (SI) in oceanography. Paris, France, *UNESCO Technical Paper* in *Marine Science,* no. 45, 53 p.

U.S. Army Corps of Engineers. 1989, Hydraulic model study for the salinity impact of the John F. Baldwin, Stockton, and Sacramento ship channel projects, dynamic salinity tests. U.S. Department of the Army, Corps of Engineers, San Francisco District *Technical Memorandum* 2, 53 p.

Walters, R.A., R.T. Cheng, and T.J. Conomos. 1985. Timescales of circulation and mixing processes in San Francisco Bay waters, in Temporal dynamics of an estuary: San Francisco Bay, Cloern, J.E. and Nichols, F.H. (eds.). *Hydrobiologia,* v. 129, p. 13-36.

Walters, **R.A.,** and J.W. Gartner. 1985. Subtidal sea level and current variations in the northern reach of San Francisco Bay. *Estuarine, Coastal and Shelf Science,* v. 21, p. 17-32.

Walters, R.A., and C. Heston. 1982. Removing tidal-period variations from time-series data using low-pass digital filters. *Journal of Physical Oceanography,* v. 12, no. 1, p. 112-115.

Warner, J.C., D.H. Schoellhamer, and J.R. Burau. 1997. A sediment pathway in the back of a nearly semi-enclosed subembayment of San Francisco Bay, California. *Proceedings, 27th International Association for Hydraulic Research,* San Francisco, California, August 10-15, 1997, v. 2, p. 1096-1101.

Weir D.J. and J. McManus. 1987. The role of wind in generating turbidity maxima in the Tay Estuary, *Continental Shelf Research,* v. *7,* p. 1315-1318.

Glossary

Baroclinic flow. Circulation driven by the pressure gradient caused by horizontal differences in salinity. The baroclinic pressure gradient increases with depth under most conditions. See appendix for more details.

Barotropic flow. Circulation that is driven by the pressure gradient caused by slope in the water surface. The barotropic pressure gradient is constant with depth. See appendix for more details.

Bathymetry. Topography of the bottom of the estuary (Kimmerer 1993).

Density Gradient. Spatial density difference.

Dispersion. The scattering of particles (or mixing of salt) or a cloud of contaminants by the combined effects of shear and transverse mixing (Fischer and others 1979).

Entrapment zone. The area of the estuary where flow convergence results in the concentration of particulate matter: this usually operates through the interaction of particle (or organism) sinking and net up-estuary flow at depth (Kimmerer 1993).

Estuarine turbidity maximum (ETM). An area of the estuary where turbidity is enhanced either by entrapment or by other mechanisms (Kimmerer 1993).

Eulerian. An Eulerian method of description uses a fixed point in space as a reference. All of the properties of interest are measured with respect to, or are referenced to, this location. Therefore, measurements are made as the fluid and its properties move past the measurement location.

Gravitational circulation. A residual, two-layer flow, in which low salinity water flows seaward in the surface layer, whereas denser, more saline water flows landward in the bottom layer; this two-layer flow results from the balance between the free surface slope acting in a down-estuary direction and the longitudinal density (salinity) gradient acting in the landward direction (Officer 1976).

Lagrangian. A Lagrangian method of description takes a fluid particle world view where all of the fluid properties of interest (temperature, salinity, suspended sediment, etc.) are measured with respect to, or referenced to, a single unique parcel of water. Therefore, a Lagrangian description goes with the flow.

Null zone. The location in the estuary at which net landward flow near the bottom ceases and all tidally averaged flow throughout the water column is seaward (Kimmerer 1993).

OBS. Acronym for optical backscatterance sensor. This sensor can be calibrated to measure suspended-solids concentrations (Downing 1983; Buchanan and others 1996).

Operational definition of the entrapment zone. The salinity range of 1 to 6 (Arthur and Ball 1980).

Practical salinity units (psu). Salinities in this report are given in practical salinity units computed based on the 1985 UNESCO standard (UNESCO 1985) for salinities greater than 2. Salinities that are less than 2 are computed as in Hill and others (1996). Salinity is a conductivity ratio; therefore, has no physical units (Millero 1993). Use of psu is in this report is for clarification.

Pressure gradient. Spatial pressure difference.

Residual. This term often represents the difference between a data value and the value predicted by a regression line or other statistical model (Kimmerer 1993). In a hydrodynamic context, residual is synonymous with tidally averaged and is used to describe processes whose time scales are longer than the tidal period (30 hours).

RMS. Acronym for root mean square: computed by squaring the values in a time series, calculating a mean value, then taking its square root.

Shear. A spatial difference (gradient) in velocity. For example, a large vertical shear indicates a large difference between surface and near-bed velocities.

Spring/neap tidal cycle. Fortnightly (period of 14 days) oscillation in tidal energy that principally results from constructive and destructive interference between the diurnal (24-hour) and semi-diurnal (12-hour) partial tides. During spring tides, the ebb and flood tides are roughly equal in magnitude; however, during neap tides, two weaker and two stronger tides occur during a roughly 24-hour period. This is known as the diurnal inequality. The largest spring-neap tidal difference occurs during the summer (~June 21) and winter (~December 21) solstices.

Stokes' drift. A Eulerian residual current that is created when the tidal variation in cross-sectional area (sea level) and the tidal currents are correlated (in phase). See the Stokes' drift section in this report.

Tidally averaged. Refers to a time series that is time averaged over a tidal cycle so that signals in the data with periods equal to or less than the tidal period are removed. This is usually accomplished through the use of a digital filter (Walters and Heston 1982).

X2. Position, measured as the distance in kilometers from the Golden Gate along the axis of the estuary, of the 2-psu near-bottom isohaline (Jassby and others 1995).